Final Draft
of the original manuscript:

Atapour, M.; Blawert, C.; Zheludkevich, M.L.:
The wear characteristics of CeO2 containing nanocomposite coating made by aluminate-based PEO on AM 50 magnesium alloy.
In: Surface and Coatings Technology. Vol. 357 (2019) 626 - 637.
First published online by Elsevier: 17.10.2018

DOI: 10.1016/j.surfcoat.2018.10.033
https://dx.doi.org/10.1016/j.surfcoat.2018.10.033

The wear characteristics of CeO_2 containing nanocomposite coating made by aluminate-based PEO on AM 50 magnesium alloy

M. Atapour[a1], C. Blawert[b], M.L. Zheludkevich[b, c]

[a] Department of Materials Engineering, Isfahan University of Technology, Isfahan 84156-83111, Iran

[b] MagIC – Magnesium Innovation Centre, Institute of Materials Research, Helmholtz Zentrum Geesthacht, Max-Plank-Str. 1, 21502 Geesthacht, Germany

[c] Faculty of Engineering, University of Kiel, Kaiserstrasse 2, 24143 Kiel, Germany

Abstract

This study examined the influence of CeO_2 nanoparticles on the wear characteristics of aluminate-based PEO coatings formed on the AM50 magnesium alloy, which was developed for the automotive industry. Sliding wear assessments were conducted on a ball-on-disk tribometer at 2N, 5N and 10N loads (against an AISI 52100 steel ball). It was found that the wear characteristics were greatly affected by the addition of CeO_2 nanoparticles, especially under intermediate and high loads. The coatings with and without CeO_2 remained intact during the sliding test at 2N. Under an intermediate load of 5 N, the coating treated in the absence of CeO_2 failed, while the one made in the presence of CeO_2 offered superior wear resistance without any signs of wear failure. Under the 10 N load, the CeO_2-free coating was completely removed and the substrate emerged, which was mainly due to a combined adhesive–abrasive wear damage mechanism; in contrast, the CeO_2-containing coating (PEO-CeO_2) offered much superior wear resistance to the Mg alloy, which was consistent with the friction coefficient data. SEM-EDS analysis of the worn surface of the steel balls also indicated that the transfer of the coating fragments to the ball surface was more intensive for the nanoparticle-free coating, as

[1] Corresponding author. Tel: +983113915735, Fax: +98 311 3912752
E-mail address: m.atapour@cc.iut.ac.ir (M. Atapour)

compared to that observed for the PEO-CeO_2 coating. Also, the appearance of some deep scoring in the worn surface of the balls could be considered as a result of the three-body abrasive wear. The superior wear resistance of the CeO_2 embedded nanocomposite coating could be mainly attributed to its lower porosity, lower roughness, and higher hardness.

Keywords: Plasma electrolytic oxidation; Wear; Nanocomposite; Mg alloy; CeO2; Friction coefficient

1- Introduction

Magnesium alloys have attracted much attention in automotive, aerospace and biomedical applications due to their high specific strength, excellent castability, good machinability, recyclability, and biocompatibility [1]. However, poor wear resistance and low corrosion resistance are two major obstacles hindering the wide usage of Mg alloys for structural applications. In recent years, considerable effort has been made to improve the performance of magnesium alloys using surface treatments and coatings [2]. A prominent approach is the plasma electrolytic oxidation (PEO) process, which is emerging as a green surface treatment due to its environmental friendliness. PEO, which is evolved from the anodizing process, is a promising candidate to improve the wear and corrosion resistance. As compared to the anodizing process,

PEO is carried out at high voltages, giving rise to the generation of short-lived micro-discharges [3]. This process is accompanied by the increased pressure and temperature at the location of discharges, and a stable ceramic coating is formed due to the activation of chemical, electrochemical and plasma reactions [4]. The properties of the resulting coatings are influenced by the substrate, electrolyte, treatment time, and current regime (AC, DC or bipolar) [5]. Among these factors, the electrolyte exerts a strong effect on the coating properties [6].

With a particular focus on the effect of the PEO coatings on Mg alloys, this study developed three main electrolyte classes including silicates, phosphates and aluminates to form the proper phases for different applications. Many investigations have been previously carried out to determine the relationship between the structure and properties of the PEO coatings on Mg alloys fabricated in these electrolytes.

Recently, various investigations have been carried out to improve the composition and optimization of the microstructure of the PEO coatings, aiming to promote industrial applications. The addition of particles to the electrolytes is considered as a new strategy to obtain new functionalities for PEO coatings. It has been reported that the size, concentration, melting point and the zeta potential of the particles are the main factors affecting the coating properties [7]. Recent advances in PEO coatings with particles have been overviewed by Lu et al. [6], concluding that the introduction of particles could be an important approach to improve the coatings properties.

The effects of the tribological properties of PEO coatings on the magnesium alloys have been the subject of several studies [2, 8], revealing that the PEO coatings are not capable of offering long-term wear resistance. However, the incorporation of various particles has been used to enhance the wear performance of PEO coatings applied on the Mg alloys. For instance, Yang et al.

[9] reported that the addition of SiC nanoparticles to the PEO coatings on the AZ91D magnesium alloy resulted in the higher hardness, which could be attributed to a remarkable enhancement in wear resistance. In another attempt, Zhang et al. [10] demonstrated that the incorporation of Al_2O_3 nanoparticles into PEO coatings which are on AZ31 alloy could significantly improve the wear resistance. They explained that the higher hardness and the denser microstructure associated with composite coatings were the main factors enhancing the wear performance. AZ31 magnesium alloy was coated with PEO coatings containing SiC nanoparticles by Vatan et al. [11], indicating that SiC-reinforced coatings exhibited a lower wear rate in comparison to those without SiC due to the rolling effect of SiC during sliding. More recently, Mingo et al. [4] fabricated AZ91/SiC composites by applying the PEO method. The results indicated that the introduction of SiC particles to the electrolyte deteriorated the wear resistance. The negative effect of the reinforcement was attributed to the relatively large particles used in their investigation

and the activation of the third-body wear mechanism due to particles removal.

Recently, rare earth compounds have received considerable attention for the surface modification of Mg alloys due to their special physical and chemical characteristics as well as their environmentally friendly nature [5]. Fabrication of composite coatings containing rare earth oxides is mostly carried out with the aim of improving corrosion resistance and mechanical properties. Ceria, CeO_2, is one of the most important rare earth oxides incorporated into PEO coatings which are on different substrates [5, 12, 13]. A considerable enhancement in the corrosion resistance was reported after PEO treatment in the silicate electrolytes containing CeO_2 particles for AZ31 [13] and AM50 [5] magnesium alloys. The incorporation of CeO_2 was found to reduce the transmission pathways for corrosive ions such as Cl^-.

Since the introduction of CeO_2 particles can effectively alter the microstructure of PEO coatings, the wear characteristics can also

be expected to change. Nevertheless, it is useful to investigate the wear performance of PEO coatings with CeO_2 on the Mg alloy substrates. However, the effect of the tribological characteristics of PEO coatings on Mg alloys fabricated in the electrolytes containing CeO_2 have not been studied in detail yet.

The aim of this study was, therefore, to develop an aluminate-based PEO coating with CeO_2 nanoparticles on the AM50 magnesium alloy in order to conduct a systematic assessment and to understand the effects of CeO_2 incorporation on the tribological performance of coatings. The wear mechanisms were discussed based on the microstructural changes resulting from the presence of CeO_2 nanoparticles. This work can provide an opportunity to produce coatings that can offer superior wear protection to Mg alloys.

2- Experimental

2.1. Material

An AM50 Mg alloy (4.74 wt% Al, 0.383 wt% Mn, 0.063 wt% Si, 0.065 wt% Zn, 0.002 wt% Fe, 0.002 wt% Cu and Mg balance) was used in this investigation and machined to produce the 25 × 25 × 4 mm substrates. Before PEO processing, the specimens were progressively ground with emery papers to 1200 grit and degreased with acetone, rinsed with distilled water, and then dried.

2.2. PEO processing

The PEO electrolyte was prepared using $NaAlO_2$ (12 g/l), Na_3PO_4 (8 g/l) and KOH (1 g/l) dissolved in distilled water. To study the role of nanoparticles, the specimens were coated in electrolytes with and without CeO_2 (5 g/L) nanoparticles (size < 5 nm, 99.95 % purity, Sigma-Aldrich). The XRD spectrum of as-received CeO_2 nanoparticles is presented in Fig. 1. PEO treatment was accomplished by applying a pulsed DC power source at a constant current density of 65 mA/cm^2 for the treatment time of 10

min. The pulse ratio was t_{on}:t_{off} = 2 ms : 18 ms. The specimens and a stainless steel tube were applied as the anode and cathode, respectively. The details of the electrolytes used for the PEO processing are presented in Table 1. To provide a uniform dispersion of nanoparticles, a magnetic stirrer and a bubbling generator were applied. The temperature was held at 20 ± 2 °C by applying a cooling system. The conductivity and pH of the electrolytes were recorded using a Metterler Toledo Inlab 730 probe and a Metrohm 691 pH meter. Based on the coating electrolytes, two names including PEO and PEO-CeO_2 were used for the coatings made in the absence and presence of CeO_2, respectively.

2.2. Characterization

The surface and cross section morphology of the coatings were assessed using a scanning electron microscope (Tescan Vega3) equipped with an energy dispersive spectrometer (EDS). Before

performing the SEM analysis, the coated specimens were embedded into resin, ground successively with 800, 1200 and 2500 grit emery papers, and then polished using the diamond paste (1 μm). X-ray diffraction technique (GIXRD, D8 Advanced Bruker AXS with the Cu Ka wavelength of 1.54056A) was applied to identify the phases present in the coatings.

In order to obtain the hardness of coatings, nano-indentation experiments were carried out on four different locations of coatings cross section. Before hardness examinations, the samples were cut, mounted and mechanically polished. Nano-indentation tests were performed using a diamond berkovich indenter. The speed of indenter during test was 1.5 μm min^{-1} at 30 mN maximum load. Also, the rates of loading and unloading were controlled to be 60 mN min^{-1}.

2.3. Wear tests

The friction and wear behavior of the coatings were evaluated using a ball on disc tribotester (TRIBOtechnic company - France), which was operating at the ambient conditions (25 ± 2 °C and 30% r.H.) with an AISI 52100 steel ball of 6 mm diameter as the static sliding counterpart.

The wear tests were implemented at three loads of 2N, 5N and 10N, with the oscillating amplitude of 10 mm and the sliding velocity of 5 mm/s for 60 minutes. These parameters were selected on the basis of the previous works of the members of our group [7, 8, 14]. The wear tracks and the worn ball surfaces were studied using SEM and EDS. All tests were repeated three times to verify their reproducibility.

2.4. Corrosion tests

The corrosion behavior of the coatings in 0.5 wt% NaCl solution was examined using a computer controlled potentiostat system (Gamry interface 1000) at room temperature. A three-electrode cell consisting of a coated specimen (as working electrode with an

exposure area of 0.5 cm2), counter electrode (a platinum mesh wire) and reference electrode (saturated Ag/AgCl) was used. Potentiodynamic polarization tests were carried out at a potential scanning rate of 0.5 mV/s started from −250 mV below the open circuit potential (OCP). The corrosion parameters were extracted by Tafel extrapolation method. Also, surface morphologies of the coated specimens after potentiodynamic polarization tests were examined using optical microscopy.

3. Results and discussion

3.1. Voltage-time characteristics

The voltage-time responses of the coatings formed in the presence and absence of CeO_2 nanoparticles were recorded and presented in Fig. 2. As seen, the voltage-time response curves indicate an almost constant potential (around 400 V) after a rapid rise in the initial stages. Very similar behavior was observed for both coatings.

3.2. Microstructure

Fig. 3 presents the SEM micrographs of PEO coatings made in the presence and absence of CeO_2 particles. A porous morphology was formed for both coatings due to the generation of discharge channels and plasma bubbles implosion during the PEO treatment. Clear differences were observed in the pore size and coating roughness of PEO and PEO-CeO_2 specimens. PEO-CeO_2 coating revealed the mean surface roughness (R_a) of 0.91 ± 0.02 μm, while the coating without CeO_2 was relatively rough with the Ra value of 1.4 ± 0.1 μm. The addition of CeO_2 nanoparticles reduced the porosity and roughness of coating, confirming the results of the previous studies [12, 15]. The pores inside PEO-CeO_2 coating were partially filled by nanoparticles. However, contrary to our finding, M. Mohedano et al. [5] reported that the roughness of the coatings was increased for the specimen with CeO_2 micro-particles. This can be explained based

on the relatively larger size (size < 5 μm) of the reinforcement particles used in that work. It can be concluded that the size of particles is the main factor controlling the roughness of the coatings. It seems that CeO_2 nanoparticles were entered into the discharge channels during PEO as a result of the forces which originated from electrical field and mechanical stirring. Di et al. [15] reported that the fused CeO_2 particles obstructed the discharge channels, consequently reducing the number of pores.

The effect of the particle size on the roughness of the PEO coatings was also reported by others. Lu et al. [7] reported that under the same condition, the roughness of the PEO coating with nano-sized SiO2 particles (12 nm) decreased compared with the coating containing micro-sized particles (1-5 μm) on magnesium alloy. In another attempt, three different sizes of Si_3N_4 particles were in-situ incorporated into alkaline- based coatings on AM50 [16]. It was found that the microstructure of the PEO coatings was not affected by Si_3N_4 addition with different sizes due to inert

incorporation of particles. It was also reported that the incorporation of some nanoparticles such as CNT [17] and SiC nanoparticles [9] decreased the roughness of PEO coatings.

According to the EDS results of the top surface of coatings (Table 2), the presence of O, Na, Mg, Al and P was confirmed for both coatings. The detection of cerium in the case of PEO-CeO_2 coating showed that CeO_2 nanoparticles had been successfully introduced into the coating, because the electrolyte was the only source for Ce.

The addition of CeO_2 nanoparticles did not reveal a pronounced effect on the average coating thickness, as evidenced in Fig. 4. The average coating thicknesses were 14 ± 3 μm and 11 ± 4 μm for the PEO and PEO-CeO_2 specimens, respectively. Meanwhile, both coatings exhibited a porous outer layer and a compact inner one, as illustrated in Fig. 4. The presence of O, Na, Mg, Al and P was confirmed for both coatings based on the EDS results of the top surface of the coatings (Table. 2). Furthermore, the detection

of cerium on the surface of PEO-CeO_2 coating indicated that CeO_2 nanoparticles had been successfully embedded into the coating.

In order to determine the distribution of nanoparticles in the coating, a cross-section elemental map of the PEO-CeO_2 specimen was obtained. As shown in Fig. 5, a uniform distribution of Ce was recorded over the whole cross-section of PEO-CeO_2 coating. A relatively even distribution of nanoparticles has also been observed by others [7, 18]. Based on the findings of Lim et al. [13], CeO_2 particles migrated toward the anode due to their negative zeta potential; then they were deposited on the surface. A similar incorporation mechanism was reported for ZrO_2 nanoparticles [19]. Apart from the zeta potential, the particle size and their melting temperature are other important factors influencing the incorporation of particles [6]. Owing to the pore size distribution of the coating, it was expected that the CeO_2 nanoparticles could be deposited into the coating via discharge

channels. The high temperature and pressure associated with spark discharges facilitated the fusion of the coating material, which was coincident with the entry of nanoparticles.

Further, it was expected that the melting of particles would not be a prevailing phenomenon during PEO because the melting temperature of CeO2 (2750 °C [5]) was higher than that of the PEO process temperature (1843–2370 °C) [20]. However, according to the binary phase diagram of the MgO-CeO_2 system [21], the formation of a mixture of MgO-CeO_2 phases could decrease the melting temperature.

For a comparative purpose, the EDS mapping analysis was employed for elemental distributions of O, Mg, Al and P on the cross section of coating made without CeO_2. As can be seen in Fig. 6, a relatively uniform distribution of elements was observed in most coating regions. By comparing Fig. 6 with Fig. 5, a similar distribution of phosphorous was displayed in the coatings with

and without CeO2. It can be deduced that the addition of CeO2 nanoparticles did not influence the distribution of phosphorous.

X-ray diffraction patterns of the coated specimens are illustrated in Fig. 7. The XRD results revealed that both coatings were composed predominantly of $MgAl_2O_4$. Also, the diffraction peaks of Mg were detected in the coatings. The presence of Mg peaks in the diffraction patterns of the coatings could be due to the lower thickness of the coatings, as compared to the X-ray theoretical depth, or the easy penetration of the X-ray through the porosity networks created [22] in the coatings. The formation of $MgAl_2O_4$ has been reported to be due to the reactions between Al_2O_3 and MgO during the high temperature sparking [23].

Additionally, the peaks of CeO_2 were identified in the XRD pattern of PEO-CeO_2 coating, which is in agreement with the SEM results. It confirmed the successful incorporation of CeO_2 nanoparticles in the PEO-CeO_2 coating.

3.3. Wear performance

The wear behavior of the coatings was assessed by sliding against an AISI 52100 steel ball. The coefficient of friction (COF) of coatings versus distance was recorded for different loads of 2N, 5N and 10N, as illustrated in Fig. 8. As can be seen, both coatings revealed the same curve shapes for the loads of 2N and 5N, where COF was raised considerably in the first 10m of testing; then, it reached a steady state condition. The steady state values of COF recorded for both coatings are summarized in Table. 3. Based on the previous works [1], the increase in the abrasive component of friction is responsible of an increase of COF in the first steps.

In the wear examinations at 10N, a distinct difference was observed between the COF curves of the coatings fabricated with and without particles. The COF of the specimen without CeO_2 particles revealed large fluctuations after about 20 minutes of sliding; this was followed by a noticeable drop to around 0.35,

which was the COF of the untreated specimen. The observation of fluctuations and a sudden drop in the COF of the PEO coating with no CeO_2 particles could be correlated to the failure and the lower load bearing capacity of this coating. As depicted in Fig. 8a, the specimen produced without CeO_2 addition revealed the lowest COF of 0.35 (approximately equal to the COF of the base metal), indicating the complete removal of the layer. The appearance of severe oscillation in the friction coefficient confirmed that the Mg alloy substrate underwent adhesive wear and stick–slip phenomena. In contrast, PEO-CeO_2 coating decreased the dynamic COF fluctuations.

Probably, filling the pores with the wear debris during the test and therefore, increasing the contact area between the wear couples could be responsible for the rise of COF at the higher loads [24].

Surface appearance of the worn surfaces depicted in Fig. 9 demonstrated that the coating without CeO_2 suffered more severe wear, as compared to the coating containing CeO_2, revealing an

increase in the wear depth with load. As can be seen, the coating incorporated with CeO_2 remained intact during the wear tests for all loads.

In order to examine the wear quantitative, the wear resistance and the average wear rate of the coatings were calculated for different loads, as reported in Fig. 10. The wear rates of the coatings containing CeO_2 (PEO-CeO_2) were lower than those for the coatings with no CeO_2 at all loads. A more pronounced difference between the wear rates was registered for the 10N load. It demonstrated that the existence of reinforcing CeO_2 nanoparticles could significantly improve the wear resistance of PEO coatings.

Fig. 11 reveals the worn tracks of PEO and PEO-CeO_2 coatings at the higher magnification. As can be seen, the extent of damage was increased with load for both coatings. While both coatings remained intact at 2N, the worn surfaces obtained at 5N and 10N were distinctly different. It seemed that both coatings offered more

resistance to the AM50 alloy against abrasive and adhesive mechanisms at the load of 2N. It should be noted that the wear resistance is a characteristic that can be controlled by the roughness and hardness of PEO coatings. The fragile nature and the low plastic flowability of PEO coatings could facilitate the occurrence of the abrasive wear [24].

Under an intermediate load of 5 N, the removal of the exterior (porous) layer of the coating without CeO_2 was observed and no catastrophic wear damage occurred. Some loose debris was observed along the edges of the wear track of this coating (Fig. 11b). However, the PEO-CEO_2 coating seemed to be more or less intact after sliding against the steel ball at 5N. PEO-CeO_2 coating did not show any considerable failure, reflecting the ability of this coating to retain wear during the test at 5N.

In the tests conducted under 10 N load, the coating prepared in the absence of CeO_2 was completely removed (Fig. 11c). After the removal of coating, the bare metal surface experienced

extensive ploughing and adhesive wear mechanisms. Furthermore, a three-body abrasive wear was also activated due to the generation of the debris which originated from the collapse of the coating during wear testing. This was corroborated by the higher wear rate of this coating. In contrast, PEO-CeO_2 coating exhibited excellent resistance against the steel ball. The formation of some ridges in the wear track of the PEO-CeO_2 coating could be attributed to the three-body-abrasive wear. This improvement could be explained according to the hardness and microstructure of the coatings. The formation of $MgAl_2O_4$ phase with high hardness in the coatings offered a higher load bearing capacity. It should be noted that the hardness of the studied coatings was measured using the nano-indentation method. For this purpose, the hardness of the dense materials was provided, whereas the studied coatings were highly porous. The hardness of the PEO coating was 329 ± 76 HV and that of the untreated substrate was about 58 HV. The hardness of the PEO-CeO_2 coating was 456 ± 48 HV too.

Higher magnification SEM studies combined with EDS analysis revealed more details about the wear features of the coatings. As shown in Fig 12, the presence of all coating elements in the worn surface of the PEO-CeO_2 coating after sliding at 10N demonstrated that the coating was still present on the surface and not removed. Fe and O were also detected, probably due to the occurrence of the abrasive wear of the steel ball and the creation of the oxide tribo-layer. This conclusion could be verified by considering the high steady state friction coefficients registered for the PEO-CeO_2 coating. Similar SEM-EDS results (not presented here) were observed for the wear tracks of PEO and PEO-CeO_2 coatings after testing at 2N and 5N loads.

In order to obtain more information regarding the wear mechanisms, the worn surface of the corresponding counterparts (steel balls) was also examined using SEM, as presented in Fig. 13. All balls exhibited a flattened surface after sliding against PEO coatings, confirming the occurrence of the abrasive mechanism

during the test. Also, the formation of some deep scoring in the worn surface of balls could be as a result of the entrapment of debris between the damaged coating and the ball surface. It should be noted that the hardness of steel balls used in this work was around 900 HV.

In comparison to the PEO coating counterpart, a completely different wear mechanism was found to occur based on the appearance of the ball surface after wear testing against the PEO-CeO_2 specimen at the 10N load. As shown in Fig. 13c, extensive ploughing and detachment of debris from the nanoparticle-free coating occurred on the surface of the ball under 10N load. However, by comparing the worn surfaces of the balls in terms of their appearance, it became evident that the balls sliding against the PEO-CeO_2 coating exhibited fewer and shallower scores under all loads. These observations were consistent with the results obtained for the wear rates. Also, the detachment of flakes from the worn surface of the coating to the

steel ball was decreased for the PEO-CeO_2 specimen, as compared to the CeO_2-free coating. This could be attributed to the fact that abrasive wear prevailed over the adhesive mechanism in the case of the PEO-CeO_2 specimen.

A close view of the surface of the steel ball tested against the coatings (Fig. 14) indicated that the extent of damage due to the three-body abrasive wear was increased for the corresponding counterpart of CeO_2-free coating. EDS results of the worn surfaces of the balls (Fig. 14b and d) demonstrated that the white wear debris observed on the ball surfaces comprised the elements from the coatings (Mg, Al, P, Na), thereby confirming the occurrence of the adhesive wear mode. Clearly, the transfer of the coating fragments was more intensive for the nanoparticles-free coating (Fig. 14a), as compared to that observed for the coating containing CeO_2 nanoparticles (Fig. 14c). The adhesively transferred materials from PEO coatings to the steel counterpart has also been reported by others [25]. It should be noted that the

roughness of PEO coatings could be of great importance for wear resistance [12]. Integration of CeO_2 nanoparticles into the coating led to the decrease of the cracks and micro-pores; also, the consequent decrease of roughness might be responsible for the wear behavior improvement.

3.4. Corrosion studies

The corrosion behavior of the coatings was assessed by potentiodynamic polarization technique in a 0.5 wt% NaCl solution after 30 min immersion in OCP condition. The corrosion plots are depicted in Fig. 15. The corrosion potential (E_{corr}) and corrosion current density (icorr) were extracted from the plots and listed in Table 4. Based on these results, the corrosion current density (i_{coor}) was decreased by CeO_2 addition. The incorporation of CeO_2 nanoparticles into the coating has led to a significant improvement in corrosion resistance as compared with corresponding PEO coating without particles. The superior corrosion resistance of the

PEO-CeO_2 coating attributed to its high compactness and the presence of small amount of ionic conducting pathways. The corroded surfaces after polarization tests demonstrated further the different corrosion aspects between the PEO and PEO-CeO2 specimens as presented in Fig. 16. This surface appearances revealed that the PEO coating suffered from severe localized corrosion attack. This is in accordance with previous findings in the case of PEO coatings on Mg [5], Ti [12] and AL [26] alloys.

It is well known that CeO_2 has a high chemical stability . Tae Seop Lim et al. [13] studied the corrosion properties of PEO coatings obtained in a CeO_2 particle-containing Na_2SiO_3-based electrolyte. They have stated that the addition of CeO_2 led to corrosion inhibition due to the formation of a barrier-type interface between coating/substrate.

Acknowledgements

The authors express their sincere thanks to the Mr. Ulrich Burmester, Mr. Volker Heitmann and Mr. Gert Wiese for their technical supports. Also, the authors are grateful to.Dr. Serdechnova for doing the XRD analyses. One of authors (M. Atapour) would like to acknowledge the National Development Fund of Iran for the financial support.

Conclusions

The influence of CeO_2 nanoparticles on the wear characteristics (against AISI 52100 steel) of aluminate-based PEO coatings formed on the AM50 magnesium alloy was investigated. The following conclusions could be drawn from this work:

1- CeO_2 nanoparticles were distributed over the whole cross section of the coating. Also, the incorporation of ceria nanoparticles reduced the porosity and roughness of the coating, resulting in the higher hardness.

2- The PEO coatings, with and without CeO_2, revealed a steady state friction coefficient throughout the whole sliding test against steel ball at small (2N) and intermediate (5N) loads. However, at

the higher test load of 10N, a sharp friction transition was recorded for the CeO_2-free coating, while the CeO_2 containing the coating exhibited a steady state regime during the whole test.

3- The coatings, in the absence and presence of nanoparticles, increased the wear resistance of the AM50 alloy at the load of 2N. At the intermediate load of 5N, while the coating without CeO_2 revealed some local damages, the PEO-CeO_2 specimen sustained the wear test. At a load of 10N, the coating prepared without CeO_2 was completely removed and the substrate emerged. However, PEO-CeO_2 coating appeared to be more or less intact after sliding against the steel ball at 10N.

5- SEM-EDS analysis of the wear tracks and the worn ball surfaces revealed that the abrasive wear mode due to the entrapment of debris between the sliding couples complete wore off CeO_2-free coating during the wear test at 10N. Furthermore, the transfer of the coating fragments was more intensive for the

nanoparticle-free coating, as compared to that observed for the coating containing CeO_2 nanoparticles.

6- PEO-CeO_2 composite coating revealed superior corrosion resistance compared to the PEO coating without CeO2, mostly due to decrease in the amount of pores and microcracks in CeO_2-containing coating.

Consequently, the results implied that the addition of CeO_2 could enhance wear resistance due to the increased hardness of PEO coatings.

References

1. Tonelli, L., et al., *Effects of graphite nano-particle additions on dry sliding behaviour of plasma-electrolytic-oxidation-treated EV31A magnesium alloy against steel in air.* Wear, 2018. **404-405**: p. 122-132.
2. Bala Srinivasan, P., et al., *Dry sliding wear behaviour of magnesium oxide and zirconium oxide plasma electrolytic oxidation coated magnesium alloy.* Applied Surface Science, 2010. **256**(10): p. 3265-3273.
3. Yerokhin, A.L., et al., *Plasma electrolysis for surface engineering.* Surface and Coatings Technology, 1999. **122**(2–3): p. 73-93.
4. Mingo, B., et al., *Corrosion and wear of PEO coated AZ91/SiC composites.* Surface and Coatings Technology, 2017. **309**: p. 1023-1032.
5. Mohedano, M., C. Blawert, and M.L. Zheludkevich, *Silicate-based Plasma Electrolytic Oxidation (PEO) coatings with incorporated CeO2 particles on AM50 magnesium alloy.* Materials & Design, 2015. **86**: p. 735-744.

6. Lu, X., et al., *Plasma electrolytic oxidation coatings with particle additions – A review.* Surface and Coatings Technology, 2016. **307, Part C**: p. 1165-1182.
7. Lu, X., et al., *Plasma electrolytic oxidation coatings on Mg alloy with addition of SiO2 particles.* Electrochimica Acta, 2016. **187**: p. 20-33.
8. Srinivasan, P.B., C. Blawert, and W. Dietzel, *Dry sliding wear behaviour of plasma electrolytic oxidation coated AZ91 cast magnesium alloy.* Wear, 2009. **266**(11–12): p. 1241-1247.
9. Yang, Y. and H. Wu, *Effects of Current Frequency on the Microstructure and Wear Resistance of Ceramic Coatings Embedded with SiC Nano-particles Produced by Micro-arc Oxidation on AZ91D Magnesium Alloy.* Journal of Materials Science & Technology, 2010. **26**(10): p. 865-871.
10. Zhang, D., et al., *A composite anodizing coating containing superfine Al2O3 particles on AZ31 magnesium alloy.* Surface and Coatings Technology, 2013. **236**: p. 52-57.
11. Nasiri Vatan, H., R. Ebrahimi-kahrizsangi, and M. Kasiri-asgarani, *Structural, tribological and electrochemical behavior of SiC nanocomposite oxide coatings fabricated by plasma electrolytic oxidation (PEO) on AZ31 magnesium alloy.* Journal of Alloys and Compounds, 2016. **683**: p. 241-255.
12. Aliofkhazraei, M., et al., *Ceria embedded nanocomposite coating fabricated by plasma electrolytic oxidation on titanium.* Journal of Alloys and Compounds, 2016. **685**: p. 376-383.
13. Lim, T.S., H.S. Ryu, and S.-H. Hong, *Electrochemical corrosion properties of CeO2-containing coatings on AZ31 magnesium alloys prepared by plasma electrolytic oxidation.* Corrosion Science, 2012. **62**: p. 104-111.
14. Chen, Y., et al., *Formation of self-lubricating PEO coating via in-situ incorporation of PTFE particles.* Surface and Coatings Technology, 2018. **337**: p. 379-388.
15. Di, S., et al., *Microstructure and properties of rare earth CeO2-doped TiO2 nanostructured composite coatings through micro-arc oxidation.* Ceramics International, 2015. **41**(5, Part A): p. 6178-6186.
16. Lu, X., et al., *Influence of incorporating Si3N4 particles into the oxide layer produced by plasma electrolytic oxidation on AM50 Mg alloy on coating morphology and corrosion properties.* Journal of Magnesium and Alloys, 2013. **1**(4): p. 267-274.
17. Kim, Y.S., et al., *Heat dissipation properties of oxide layers formed on 7075 Al alloy via plasma electrolytic oxidation.* Surface and Coatings Technology, 2015. **269**: p. 114-118.
18. Yang, J., et al., *Microstructure and corrosion behavior of Ca/P coatings prepared on magnesium by plasma electrolytic oxidation.* Surface and Coatings Technology, 2017. **319**: p. 359-369.
19. Arrabal, R., et al., *AC plasma electrolytic oxidation of magnesium with zirconia nanoparticles.* Applied Surface Science, 2008. **254**(21): p. 6937-6942.
20. Lee, K.M., et al., *Evaluation of plasma temperature during plasma oxidation processing of AZ91 Mg alloy through analysis of the melting behavior of incorporated particles.* Electrochimica Acta, 2012. **67**: p. 6-11.
21. Preda, M. and R. Dinescu, *THERMAL EQUILIBRIA IN BINARY-SYSTEMS MGO-CEO2, CAO-CEO2, SRO-CEO2, BAO-CEO2.* Revue Roumaine de Chimie, 1976. **21**(7): p. 1023-1030.
22. Curran, J.A. and T.W. Clyne, *Porosity in plasma electrolytic oxide coatings.* Acta Materialia, 2006. **54**(7): p. 1985-1993.
23. Li, X., X. Liu, and B.L. Luan, *Corrosion and wear properties of PEO coatings formed on AM60B alloy in NaAlO2 electrolytes.* Applied Surface Science, 2011. **257**(21): p. 9135-9141.
24. Sharifi, H., et al., *Tribological properties of PEO nanocomposite coatings on titanium formed in electrolyte containing ketoconazole.* Tribology International, 2016. **102**: p. 463-471.
25. Wang, Y.M., et al., *Tribological behavior of microarc oxidation coatings formed on titanium alloys against steel in dry and solid lubrication sliding.* Applied Surface Science, 2006. **252**(8): p. 2989-2998.

26. Arunnellaiappan, T., et al., *Fabrication of corrosion-resistant Al2O3–CeO2 composite coating on AA7075 via plasma electrolytic oxidation coupled with electrophoretic deposition.* Ceramics International, 2016. **42**(5): p. 5897-5905.

Table Captions

Table 1. Characteristics of the PEO electrolytes used in this investigation.

Table 2. EDS results of the top surface of coatings (wt%)

Table 3. Steady state values of COF recorded for both coatings

Table 4. The extracted corrosion parameters from the polarization curves using Tafel extrapolation method.

Figure Captions

Fig. 1. X-ray diffraction pattern of CeO_2 powders used in this work.

Fig. 2. Voltage vs. Time plots during the PEO treatment in the presence and absence of CeO_2.

Fig. 3. SEM micrographs of PEO coatings made in the presence and absence of CeO_2 particles. (a) PEO and (c) PEO-CeO_2; Higher magnification image of (b) PEO and (d) PEO- CeO_2.

Fig. 4. SEM images of the cross section of PEO coatings (a) PEO, (b) PEO-CeO_2.

Fig. 5. Elemental map of PEO-CeO_2 specimen.

Fig. 6. Cross-section elemental map of the PEO coating whithout CeO2 nanoparticles obtained by EDS.

Fig. 7. X-ray diffraction patterns of the coated specimens

Fig. 8. Variation of friction coefficient with sliding distance for (a) PEO and (b) PEO-CeO2 coatings under 2N, 5N and10 N loads.

Fig. 9. SEM image showing the appearance of the worn surfaces: (a) PEO and (b) PEO-CeO_2

Fig. 10. Wear rate of both specimens under different loads.

Fig. 11. SEM micrographs of the wear track of coatings after sliding against steel ball under different loads.

Fig. 12. SEM–EDS analysis of the worn surface of PEO-CeO2 specimen after sliding against steel ball under 10N load.

(a) Micrograph illustrating the zone of EDS analysis. (b) and (c) EDS spectra of box regions in (a).

Fig. 13. Surface morphology of the steel ball counterparts slid against coated specimens under different loads of 2N, 5N and 10N.

Fig. 14. High magnification SEM images and EDS analyses of the steel balls after testing under 10N load. (a) PEO coating, (b) EDS spectrum of the box region in (a), (c) PEO-CeO_2 coating, (d) EDS spectrum of the box region in (c).

Fig. 15. Polarization curves of the coated samples after 30 min immersion in 0.5 wt% NaCL.

Fig. 16. Surface morphologies of coated specimen after polarization tests (a) PEO and (b) PEO-CeO_2.

Table 1

Sample	KOH (g/l)	$NaAlO_2$ (g/l)	Na_3PO_4 (g/l)	CeO_2 (g/l)	Conductivity (mS cm^{-1})	pH
PEO	1	12	8	0	23.7	12.5
PEO/CeO2	1	12	8	5	23.2	12.6

Table 2

Coating	O	Na	Mg	Al	P	Ce
PEO	18	0.7	24	46	11	0
PEO-CeO_2	20	0.6	28	32	8	8

Table 3

Coating	2N	5N	10N
PEO	0.53 ± 0.01	0.6±0.0.01	0.35 ± 0.05
PEO-CeO_2	0.48±0.0.02	0.55±0.0.02	0.63±0.0.02

Table 4

Coating	E_{corr} vs Ag/AgCl (mV)	I_{corr} (nA cm-2)
PEO	1523 ± 6	541 ± 21
PEO-CeO_2	1522 ± 14	24 ± 5

Figure 1

Click here to download high resolution image

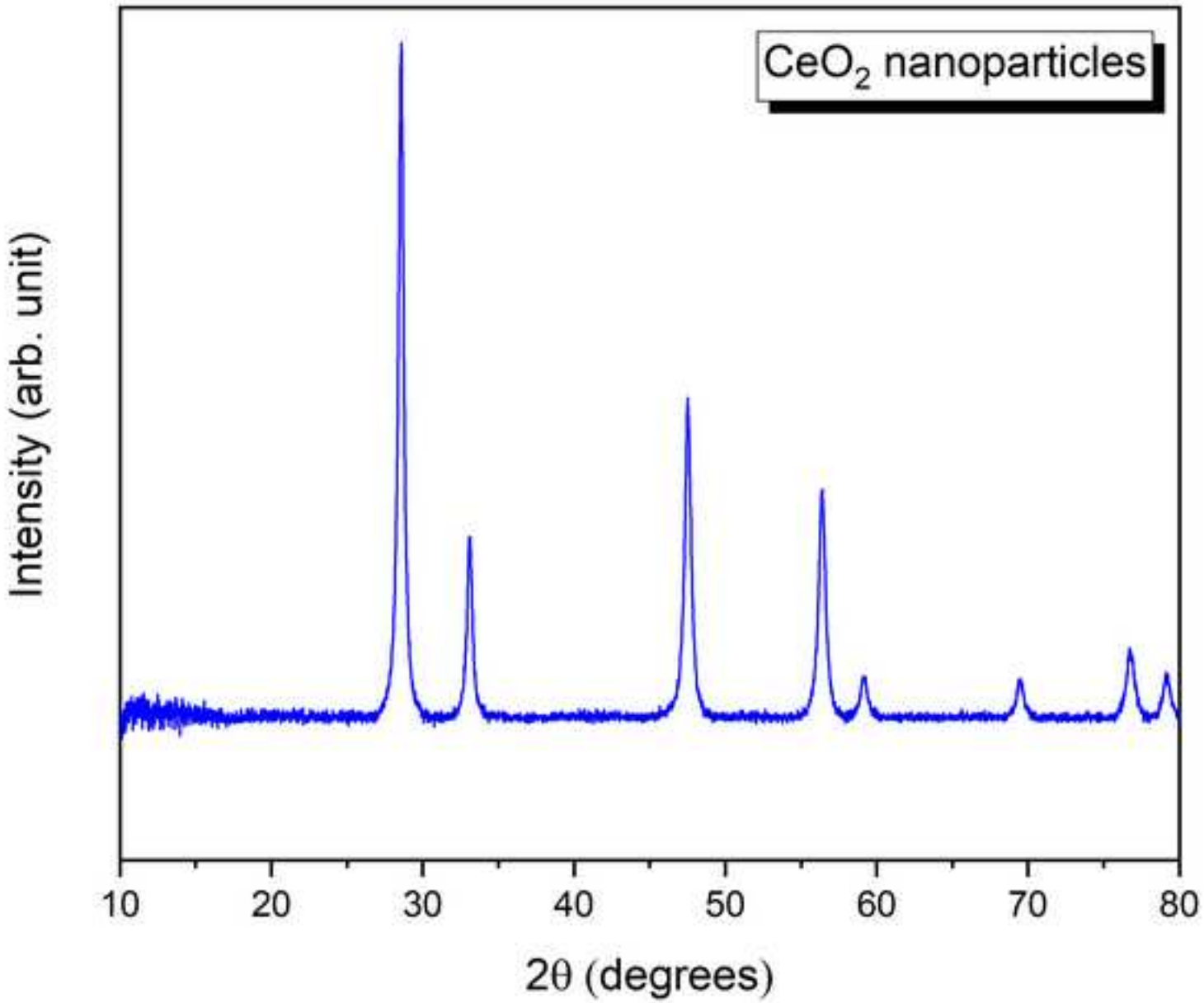

Figure 2

Click here to download high resolution image

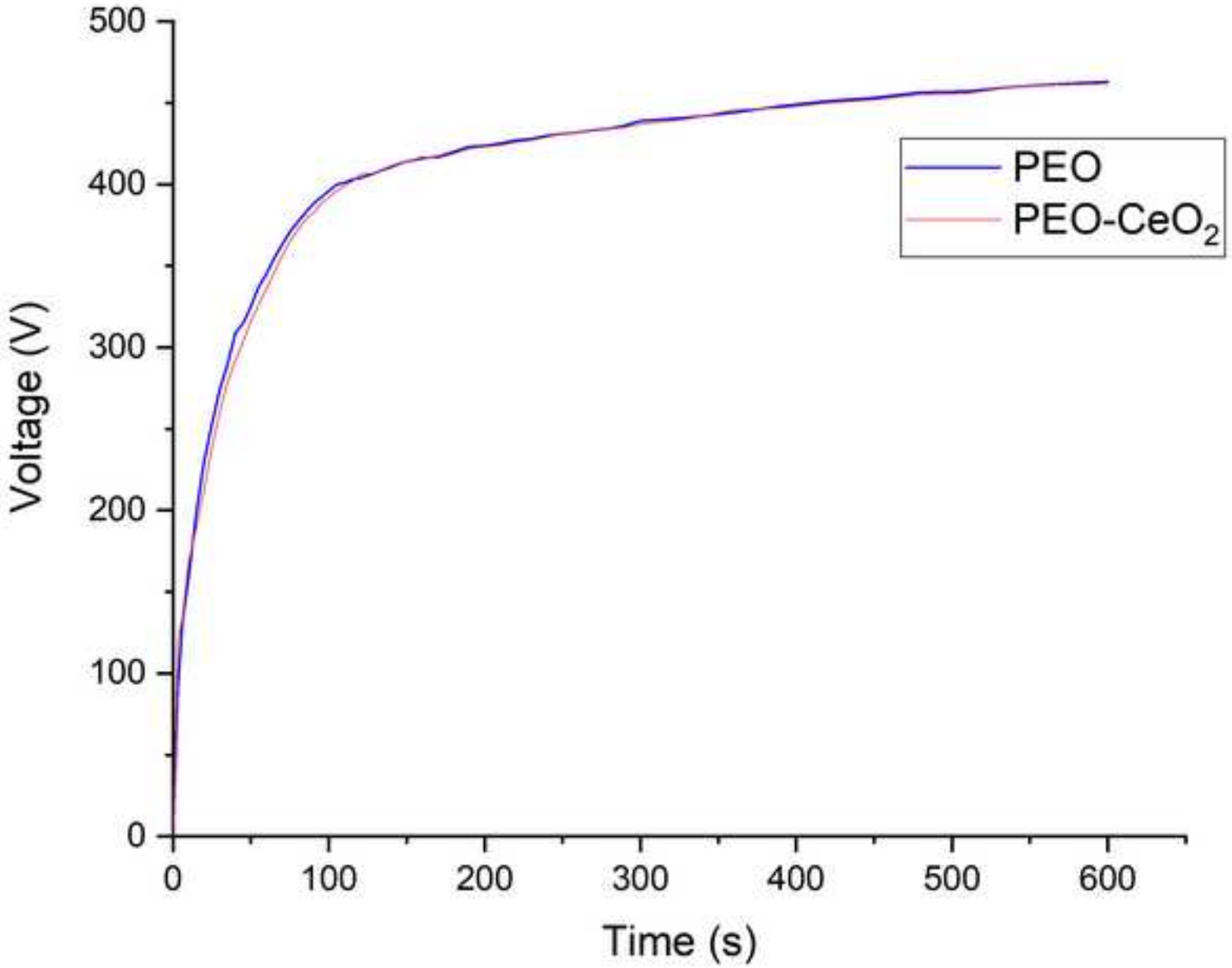

Figure 3

Click here to download high resolution image

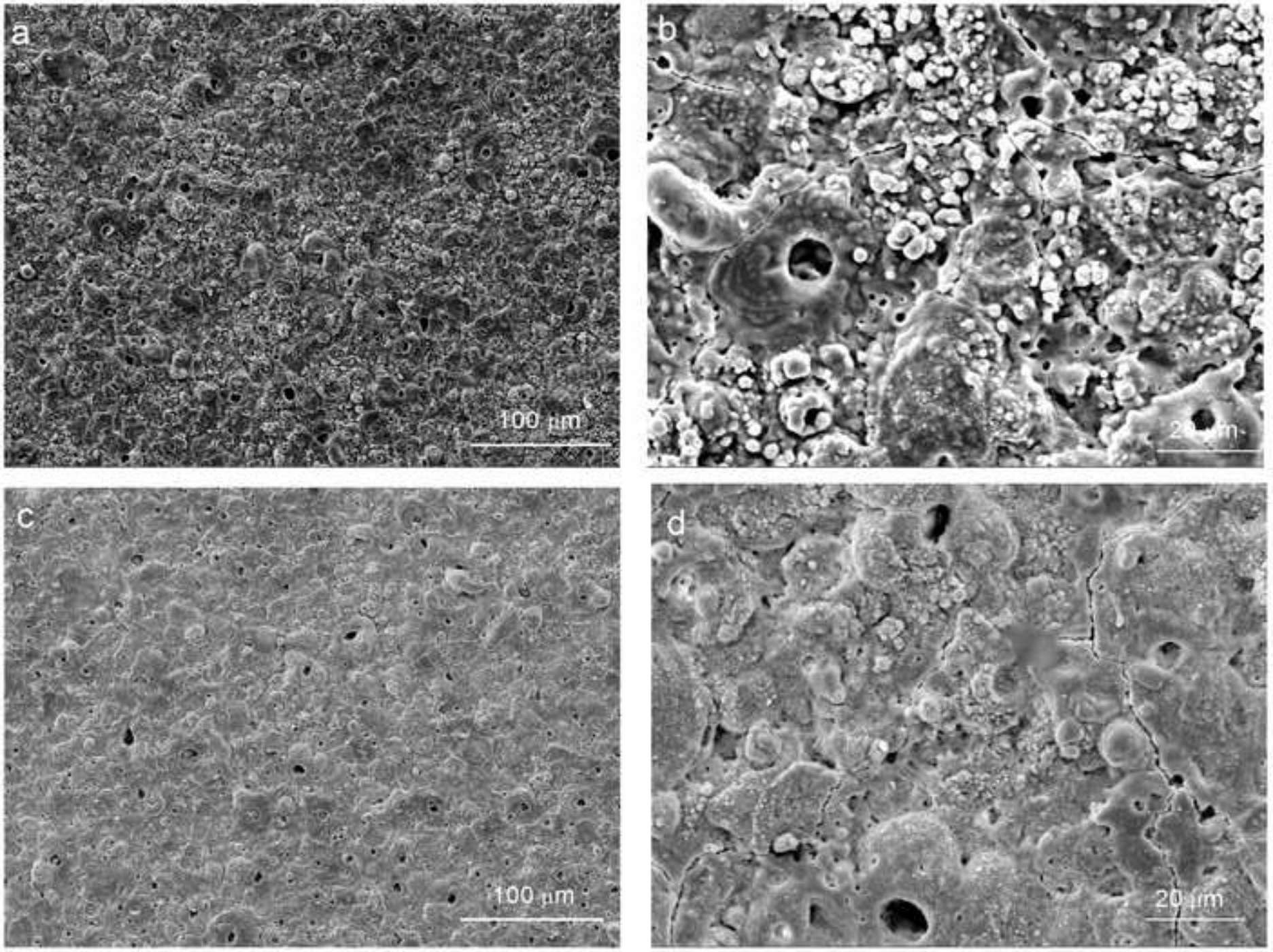

Figure 4

Click here to download high resolution image

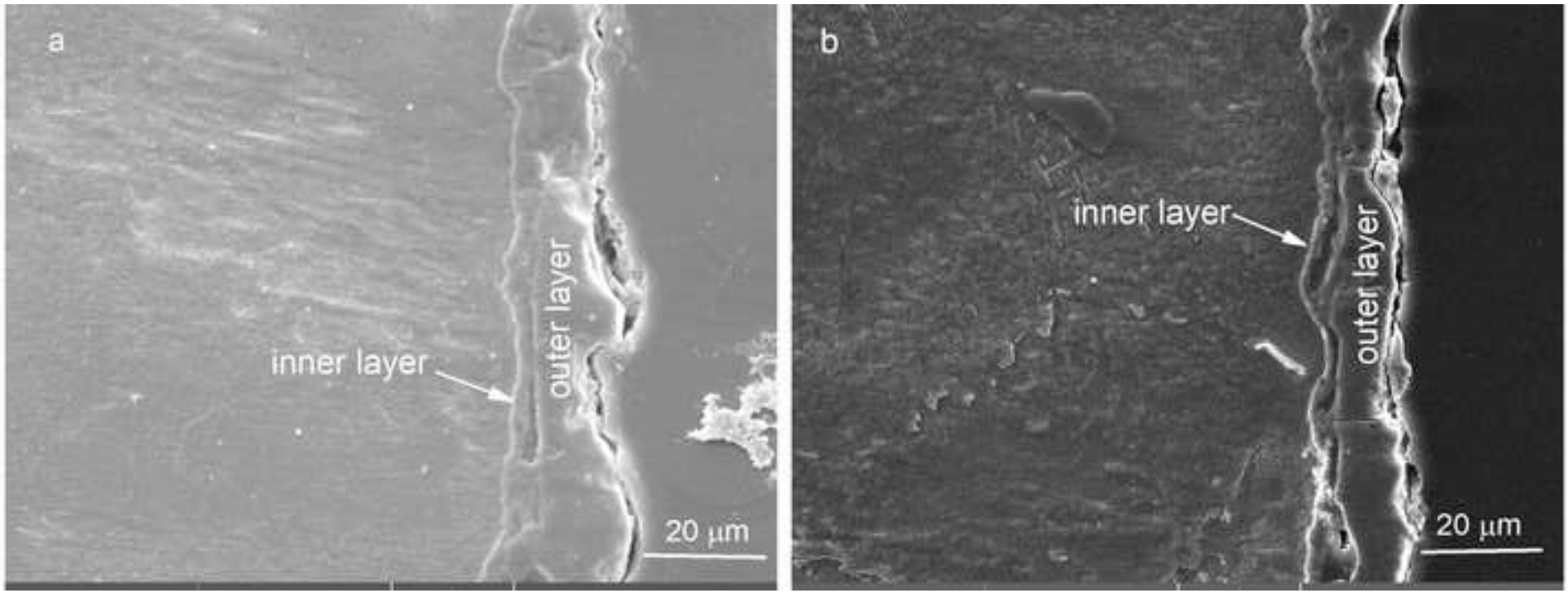

Figure 5

Click here to download high resolution image

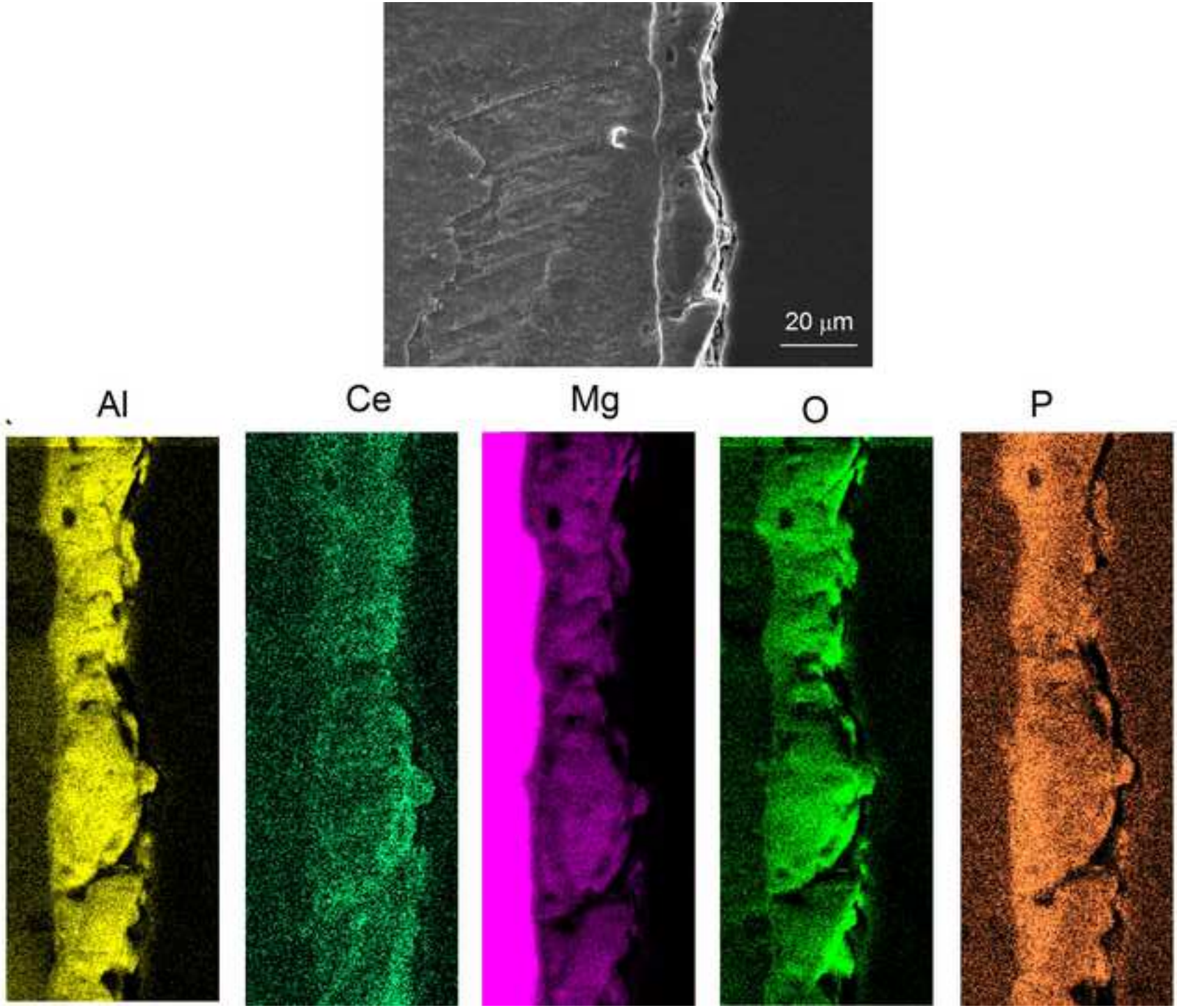

Figure 6

Click here to download high resolution image

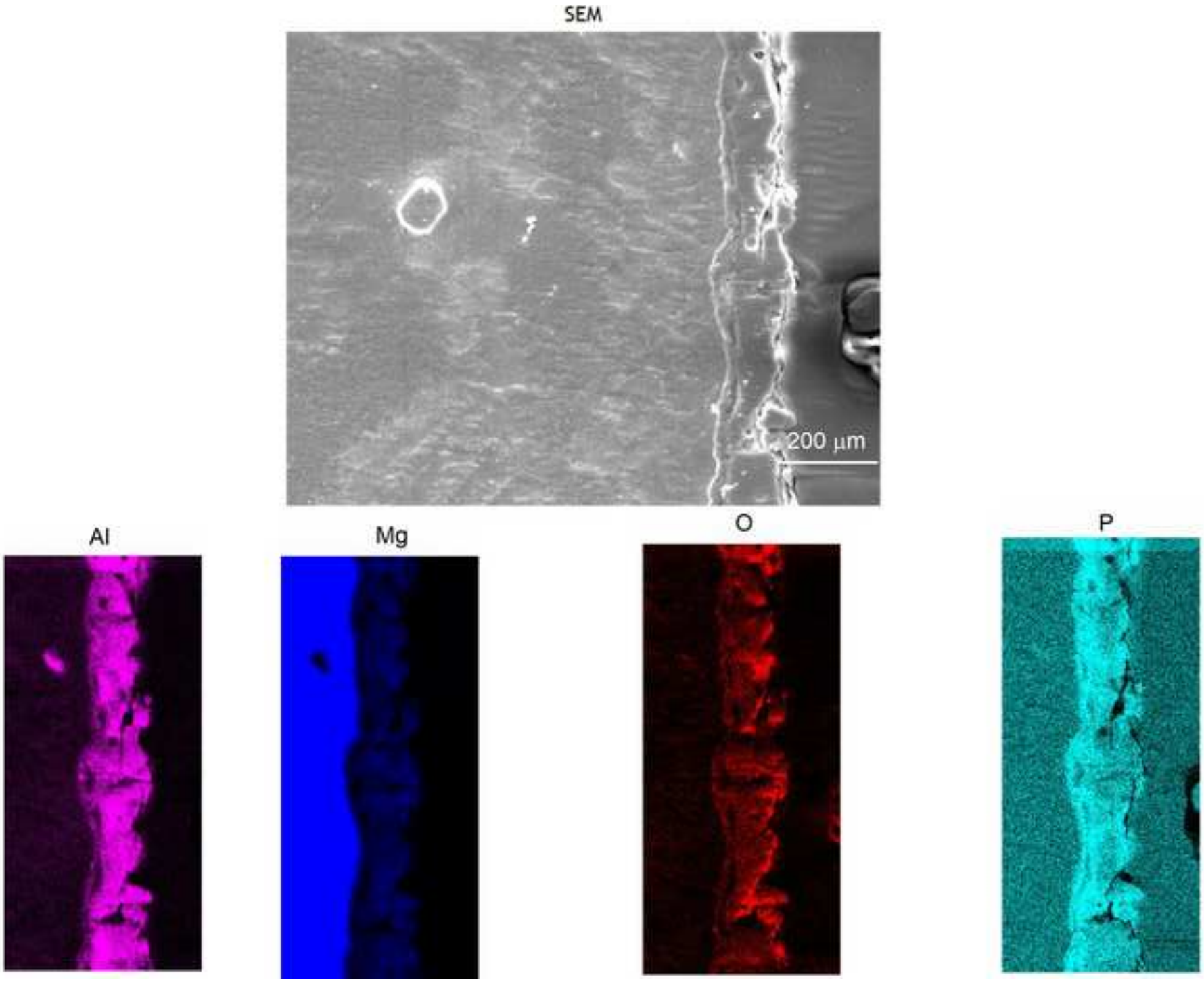

Figure 7a

Click here to download high resolution image

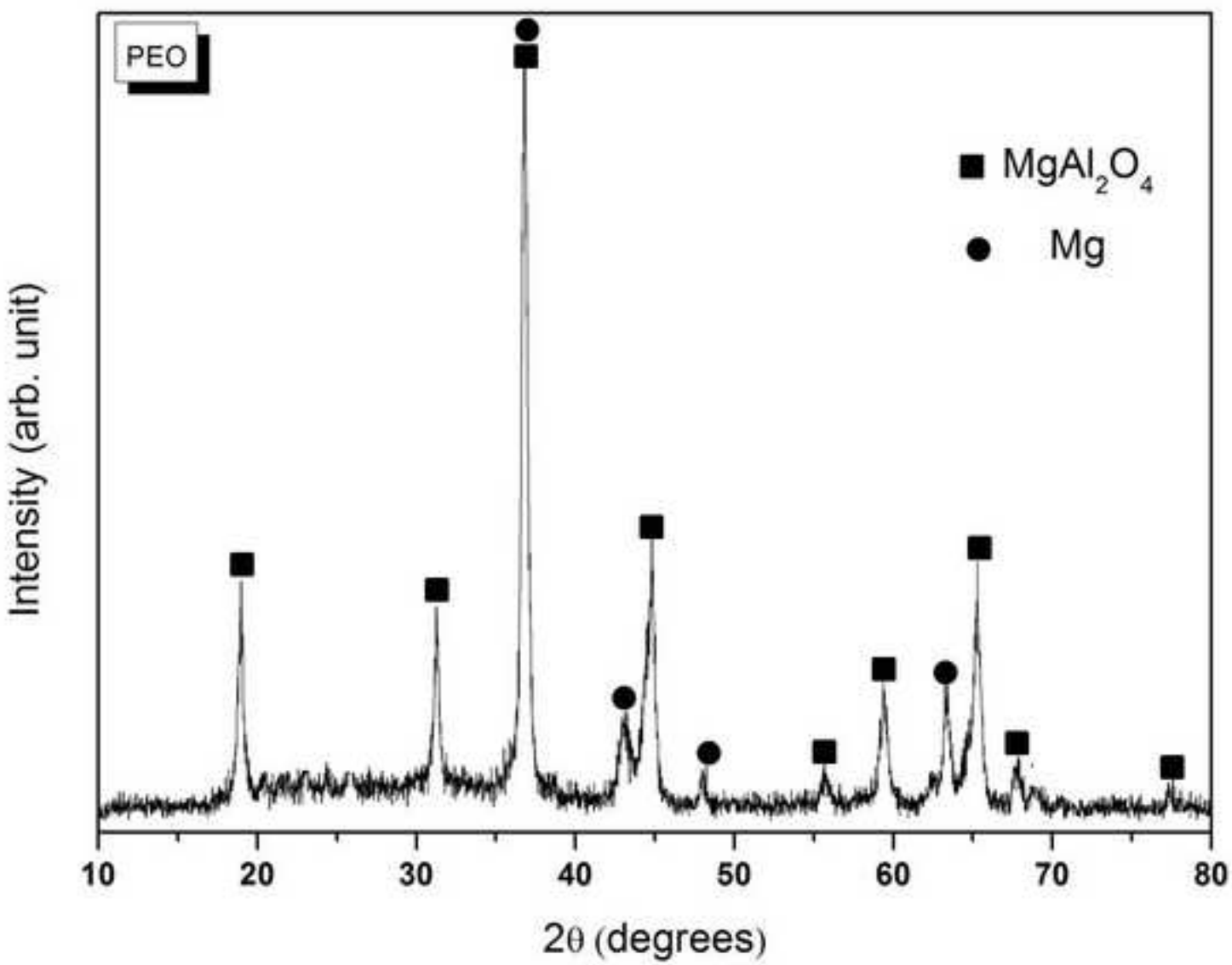

Figure 7b

Click here to download high resolution image

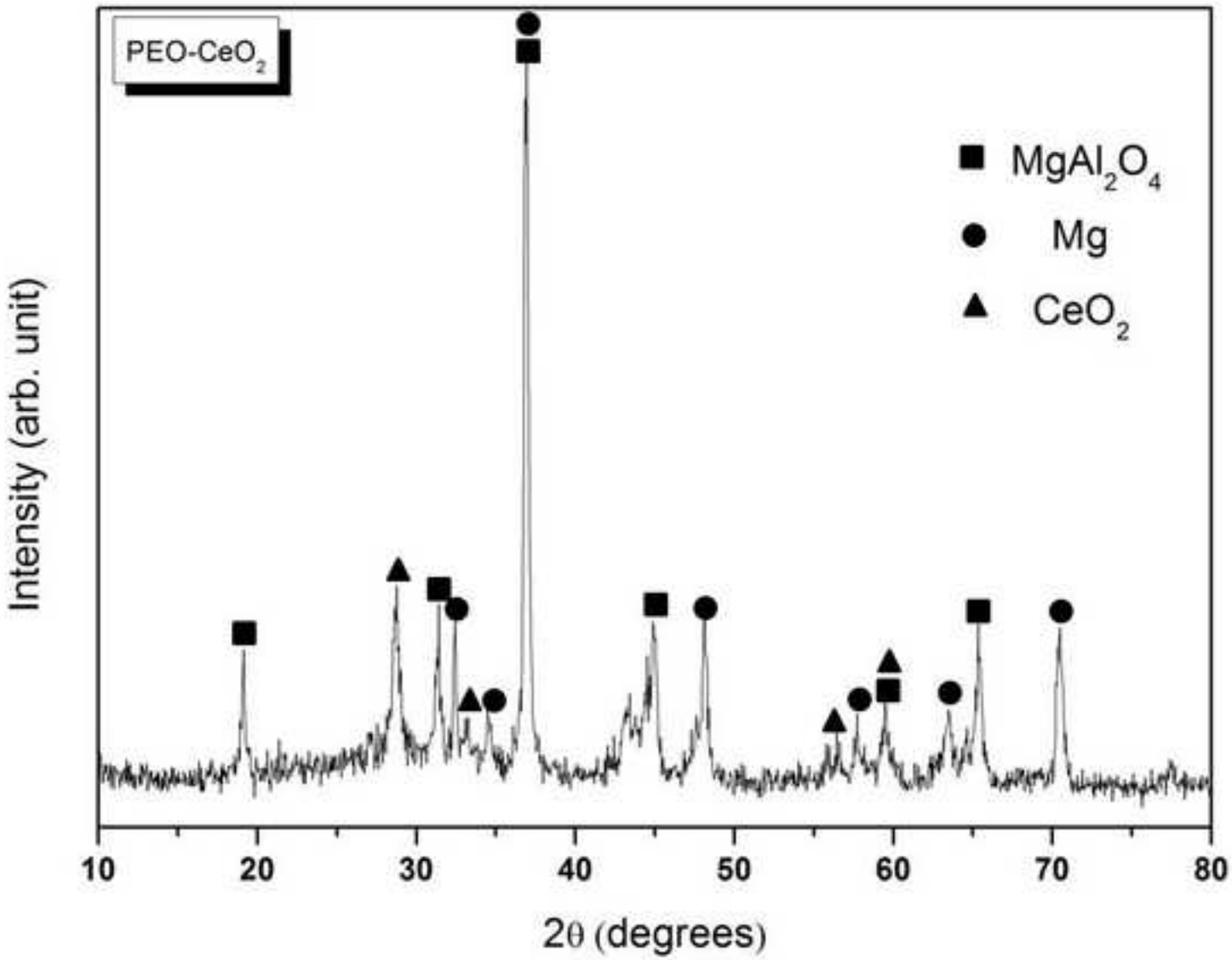

Figure 8a

Click here to download high resolution image

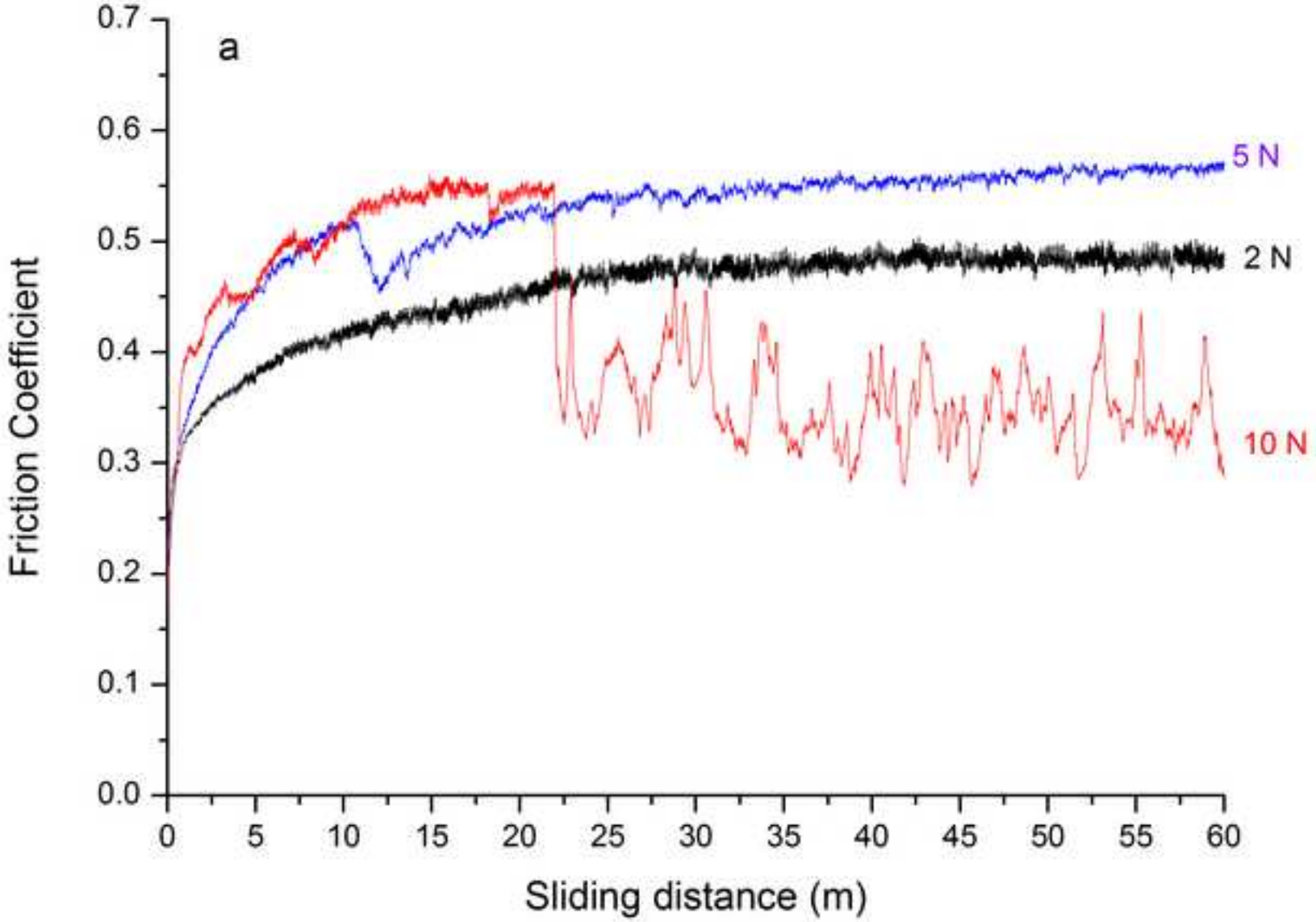

Figure 8b

Click here to download high resolution image

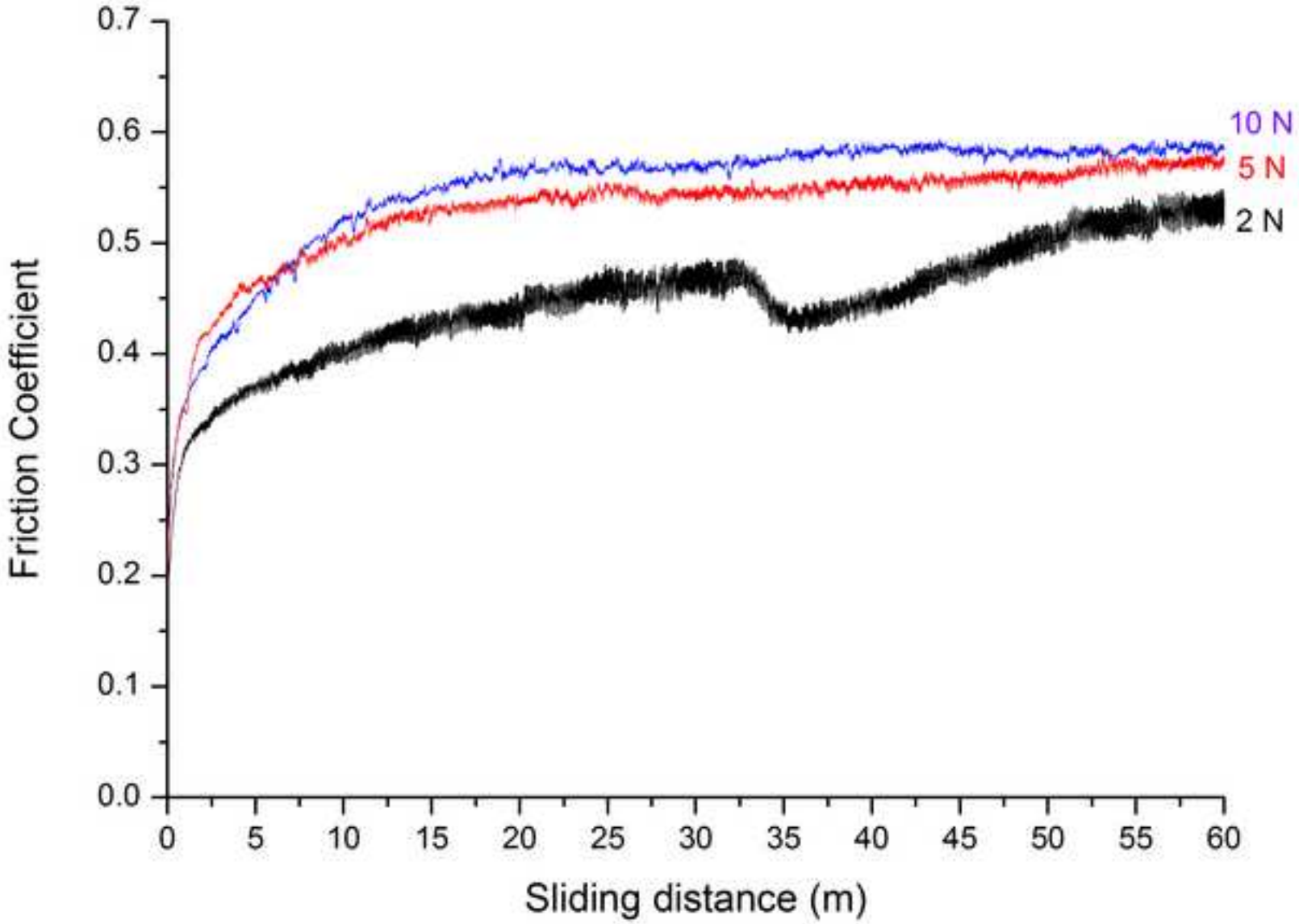

Figure 9

Click here to download high resolution image

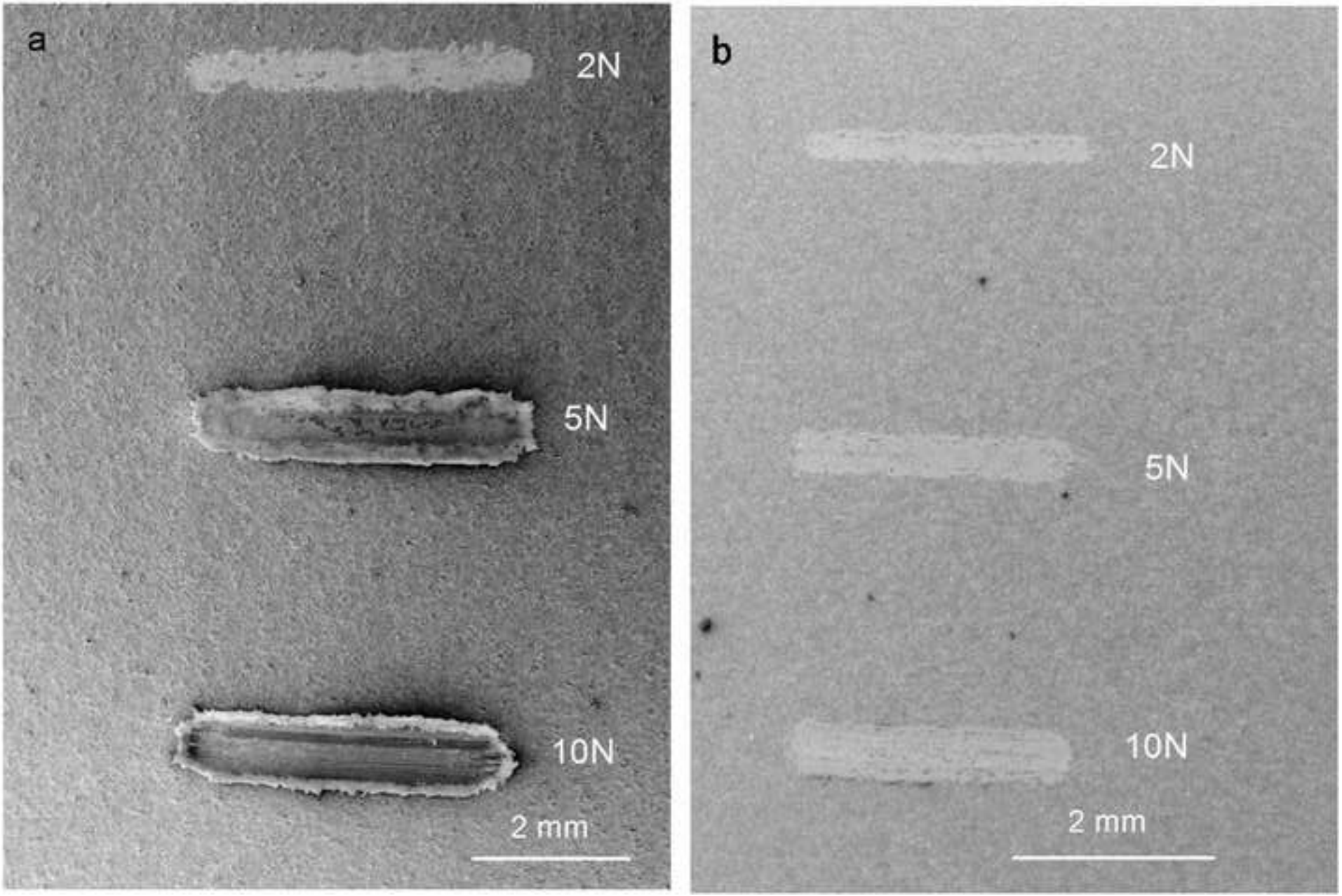

Figure 10

Click here to download high resolution image

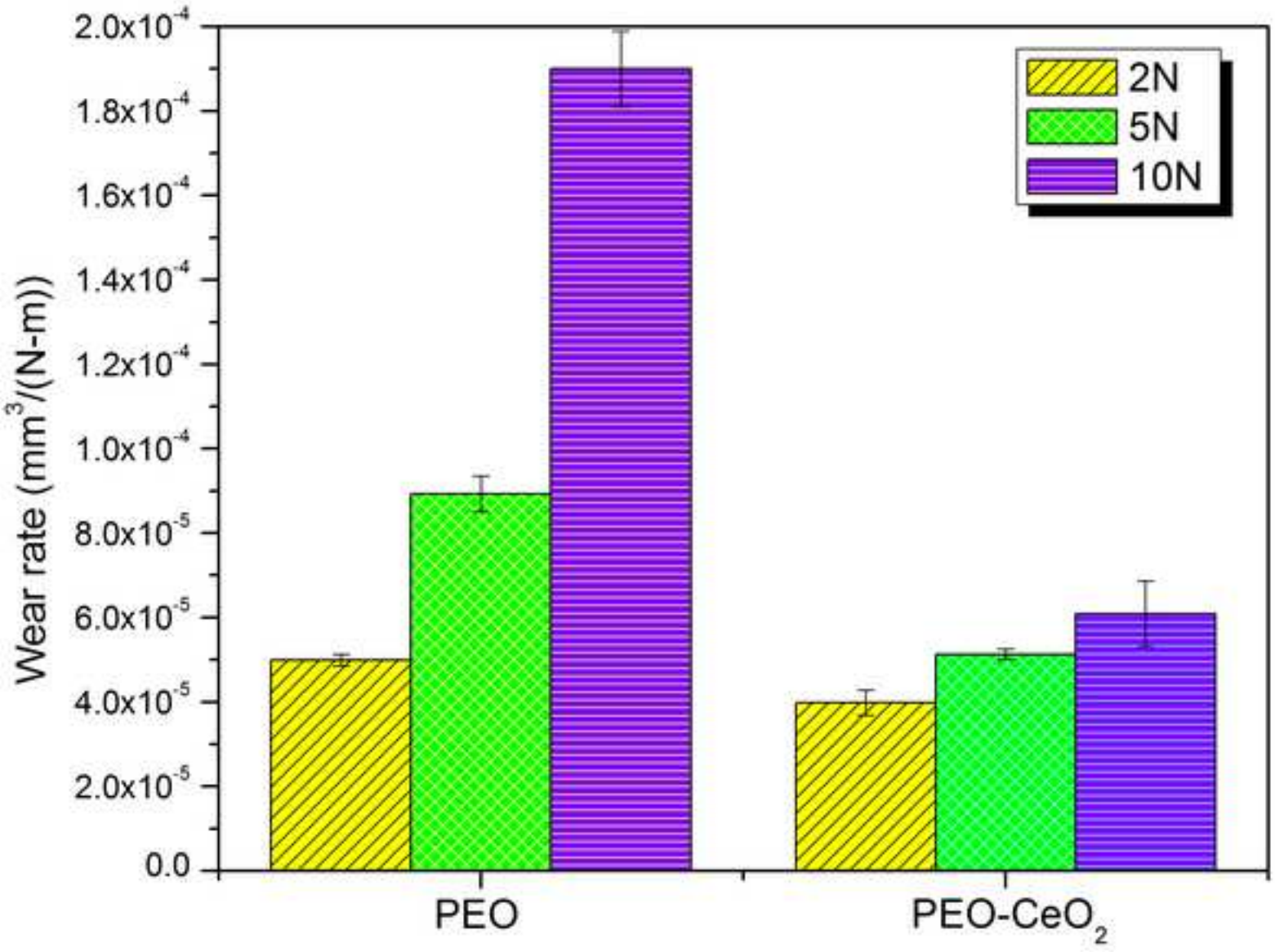

Figure 11

Click here to download high resolution image

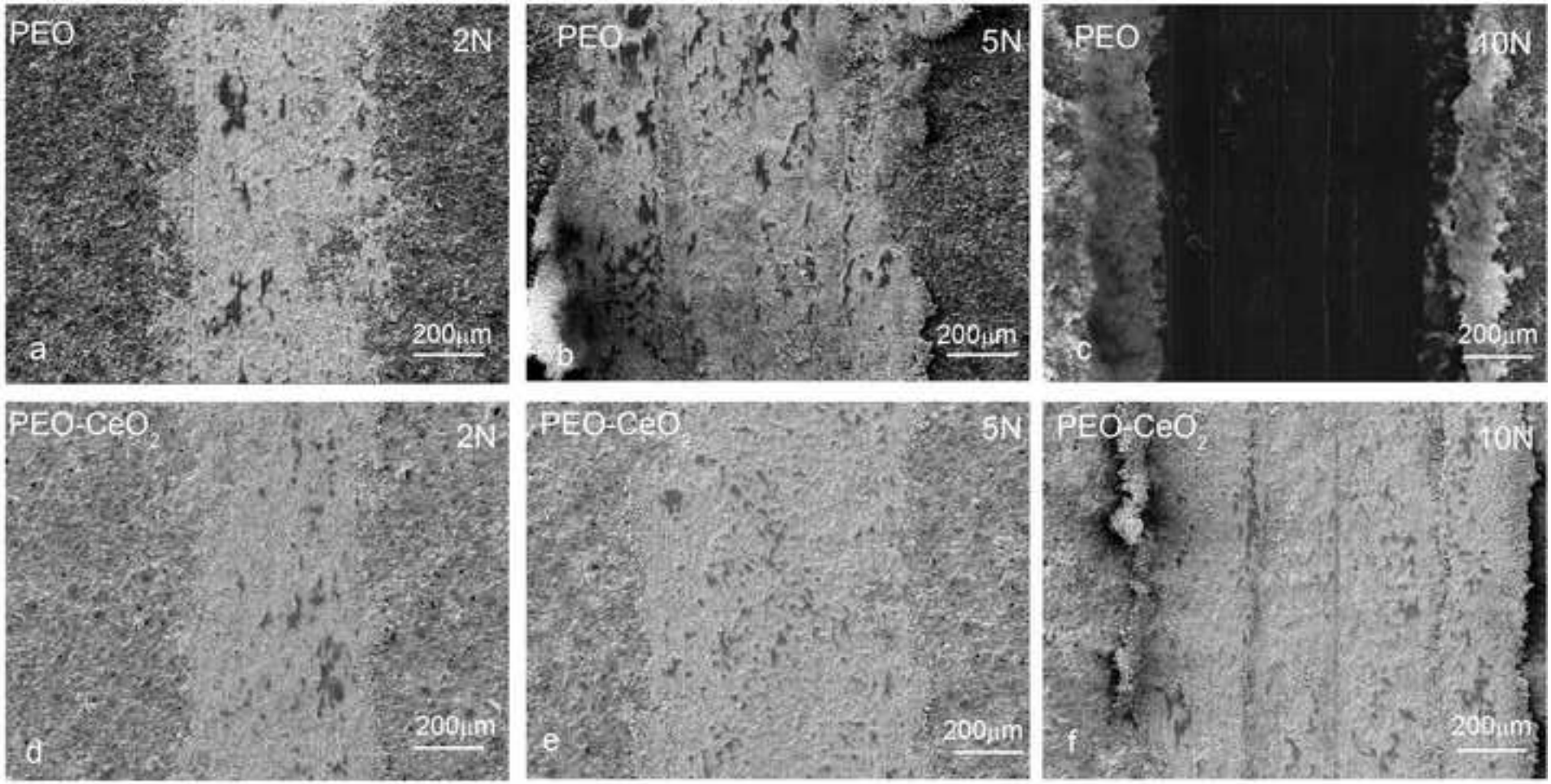

Figure 12a

Click here to download high resolution image

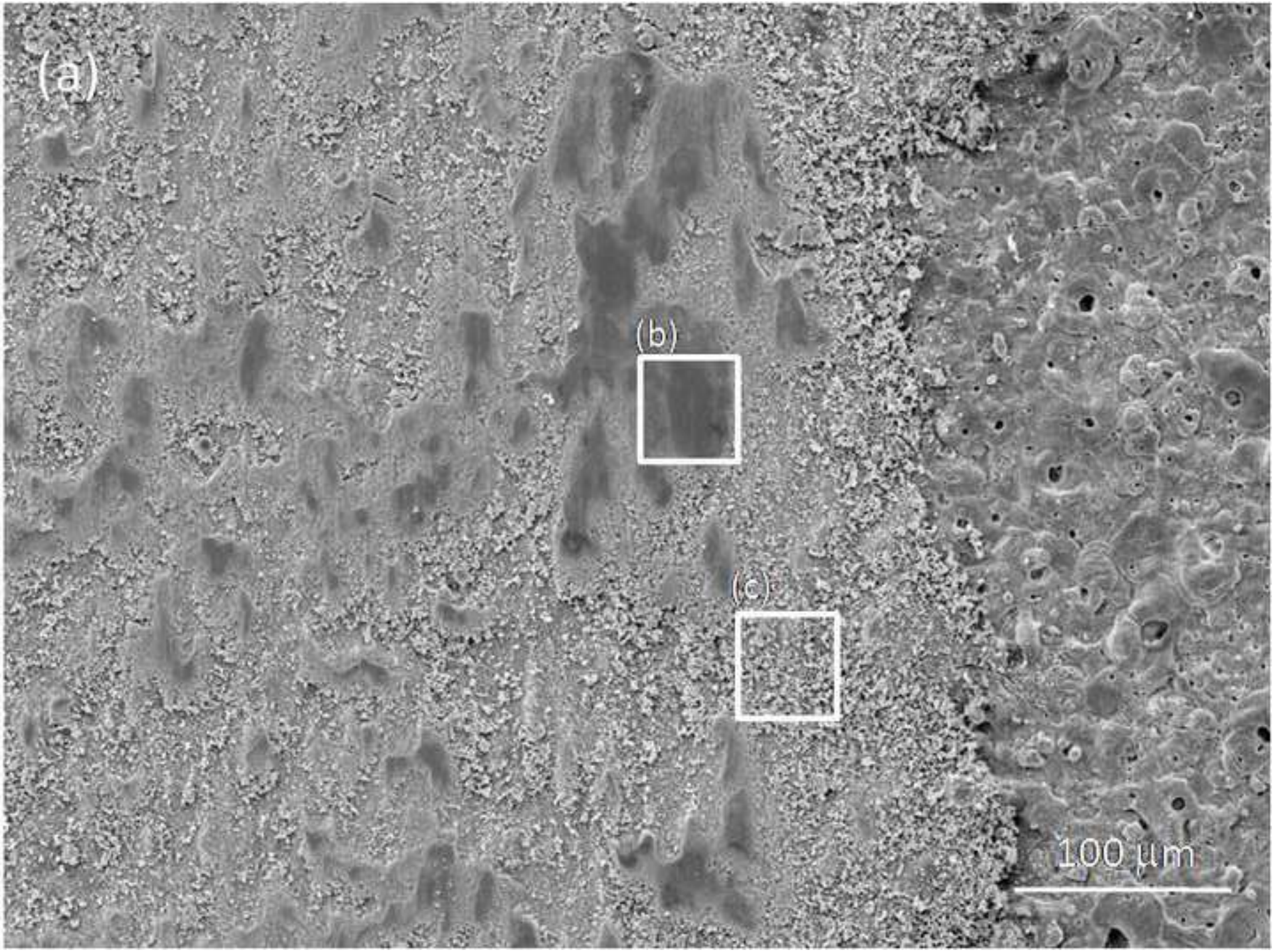

Figure 12b

Click here to download high resolution image

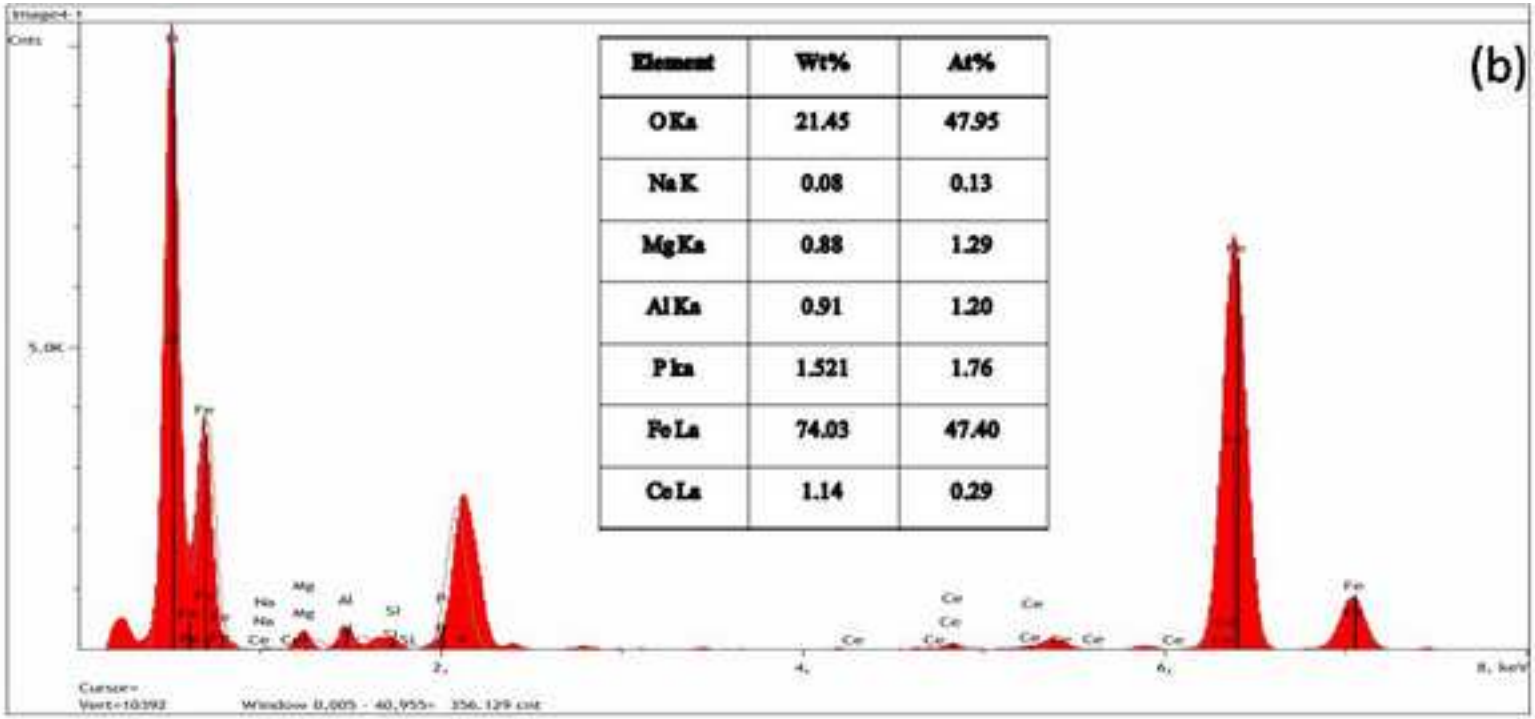

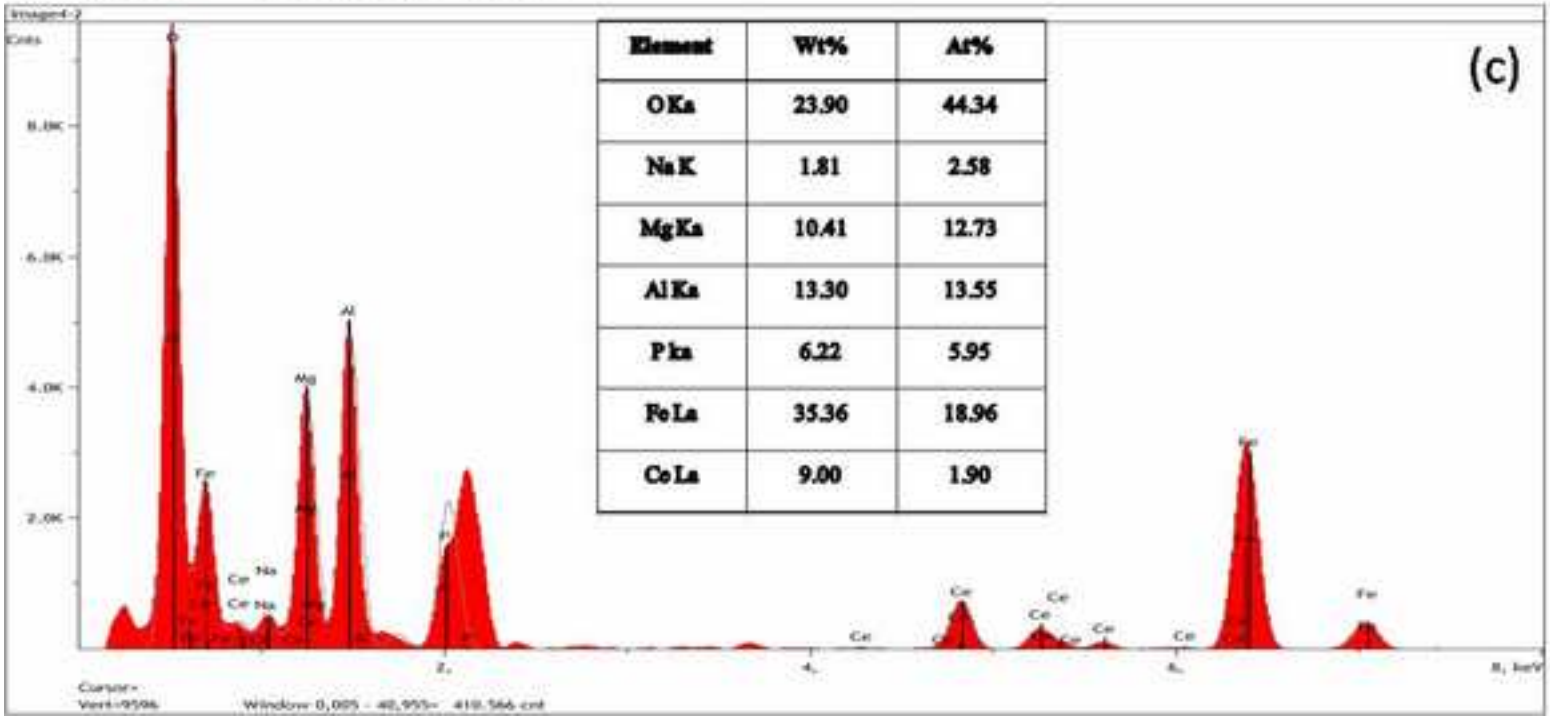

Figure 13

Click here to download high resolution image

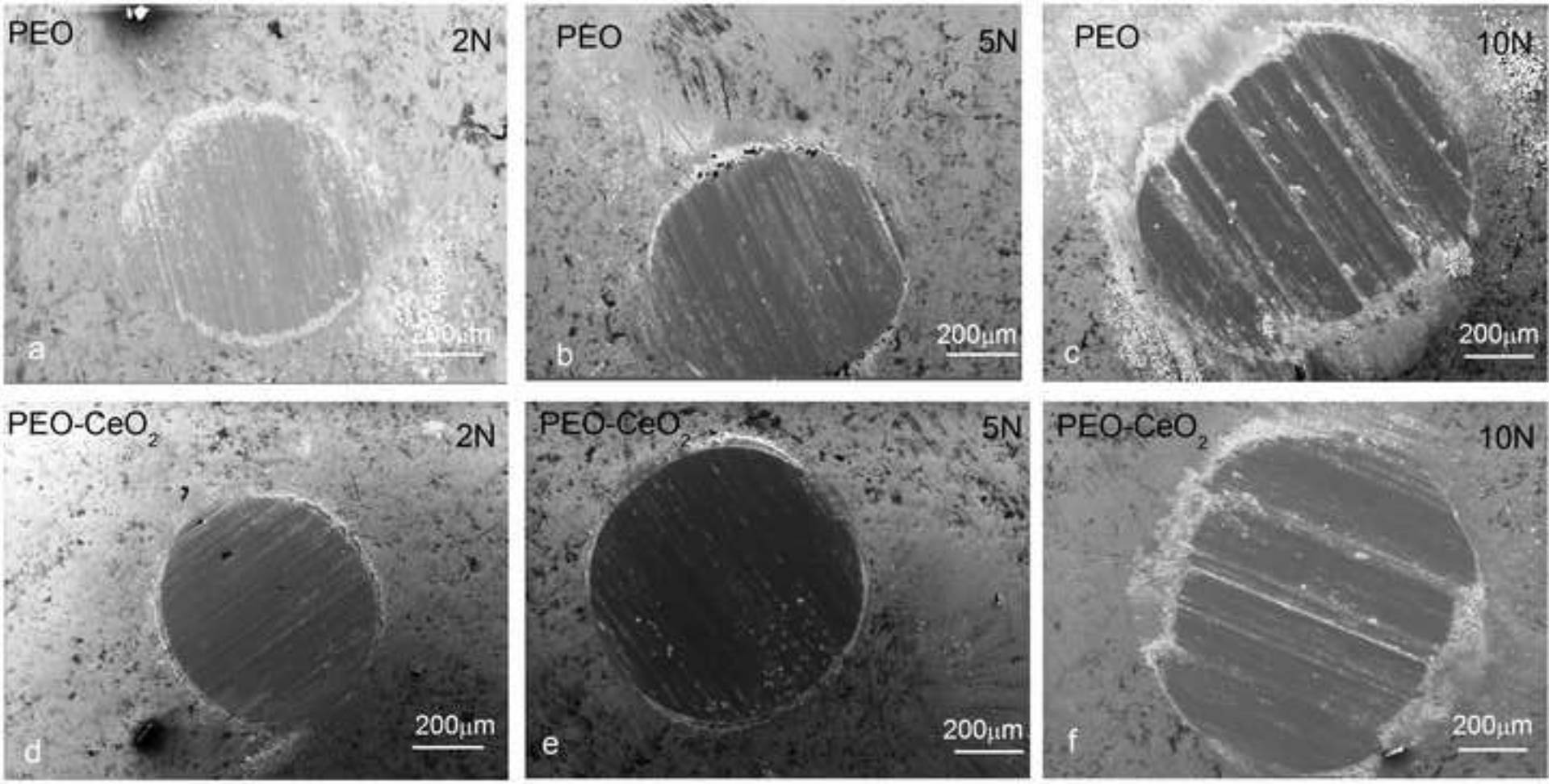

Figure 14ab

Click here to download high resolution image

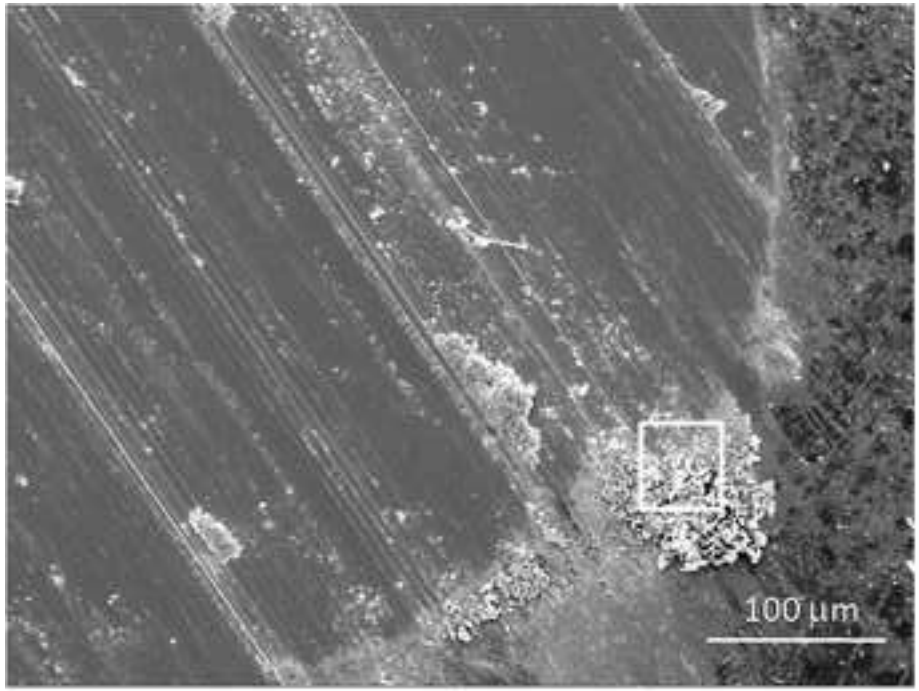

Element	Wt%	At%
O Ka	23.25	44.22
Na K	0.46	0.61
Mg Ka	10.18	12.74
Al Ka	9.28	10.47
P ka	2.77	2.14
Cr	0.97	0.57
Fe La	53.09	29.25

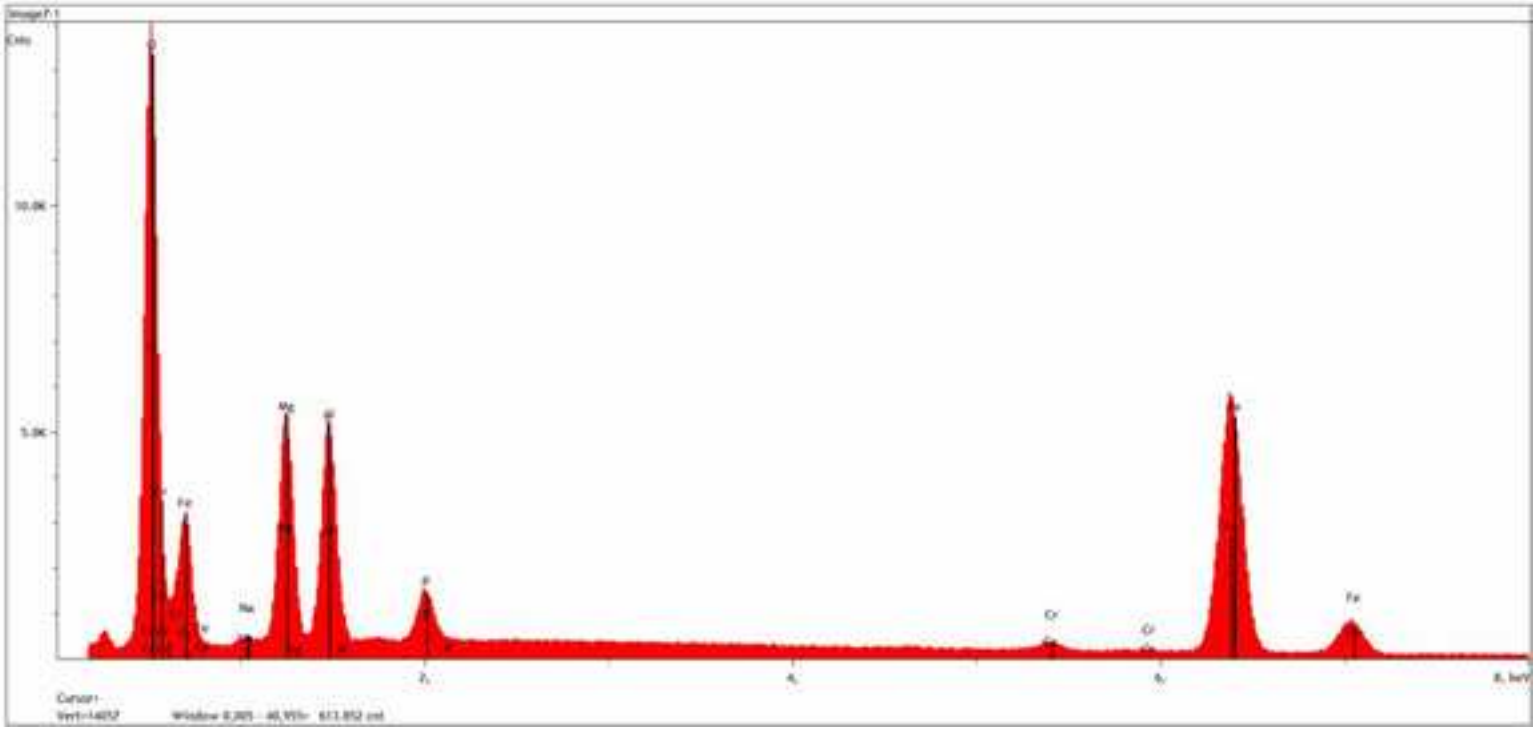

Figure 14cd

Click here to download high resolution image

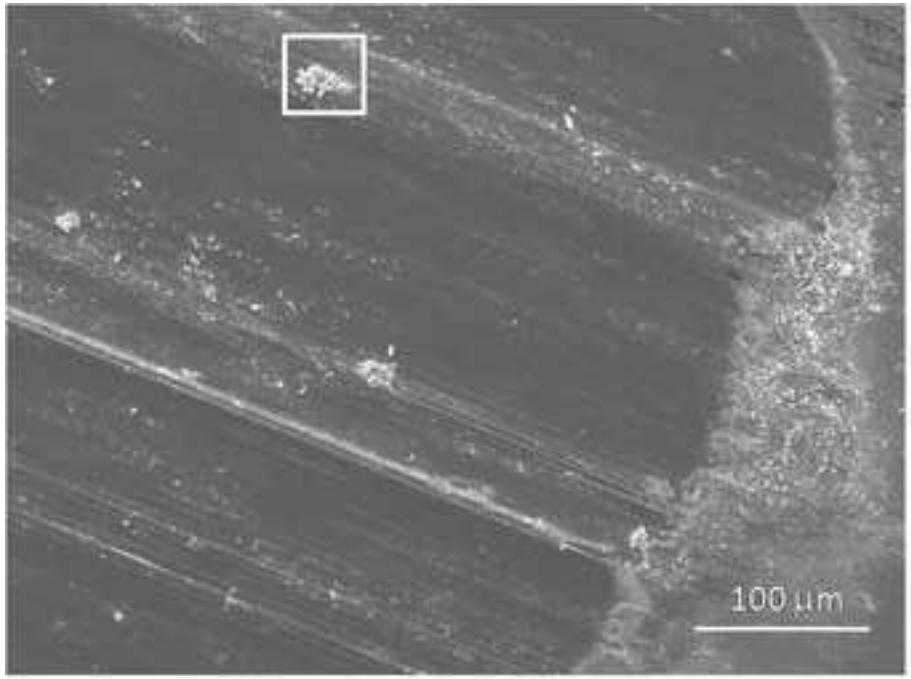

Element	Wt%	At%
O Ka	12.98	32.02
Na K	0.09	0.16
Mg Ka	3.69	5.99
Al Ka	3.55	5.19
P ka	0.76	0.96
Cr	1.23	0.95
Fe La	77.15	54.57
Ce La	0.56	0.16

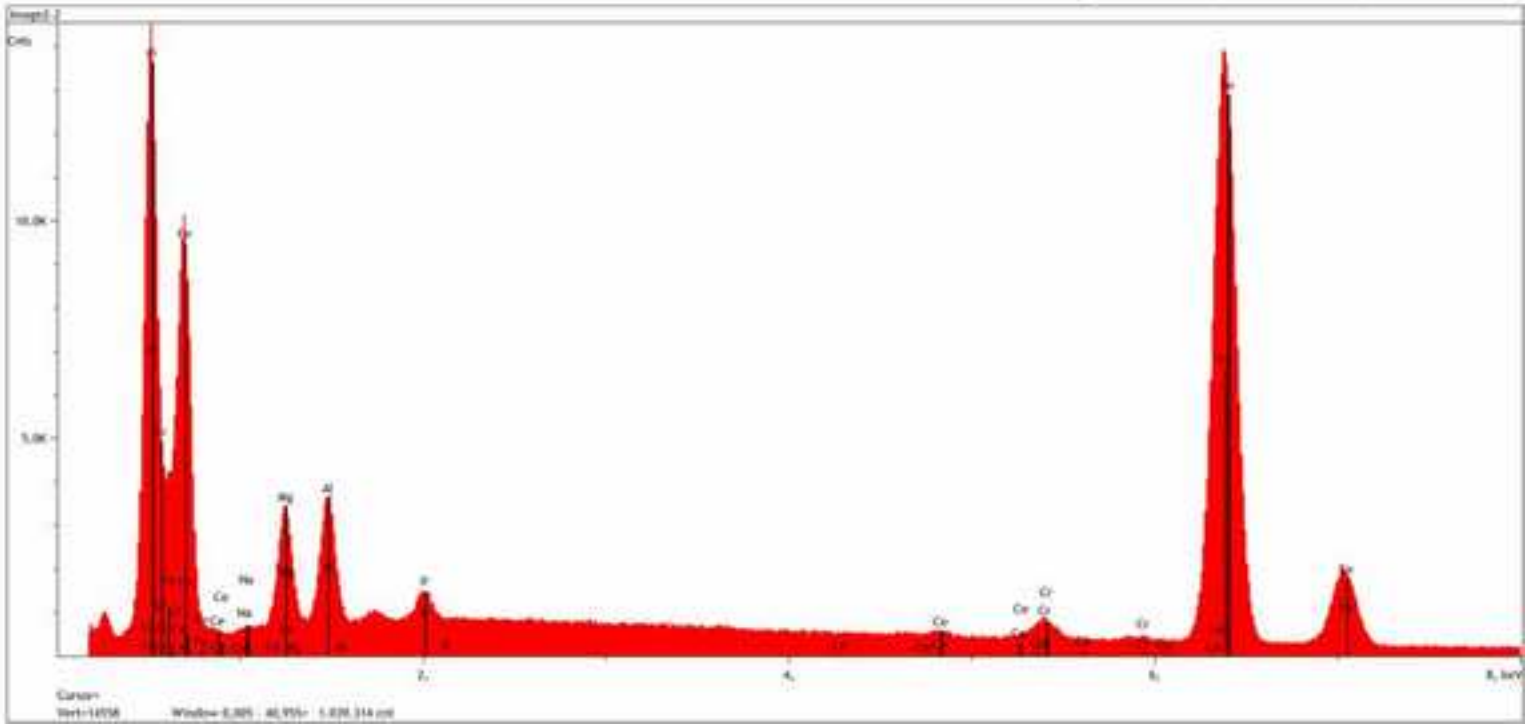

Figure 15
Click here to download high resolution image

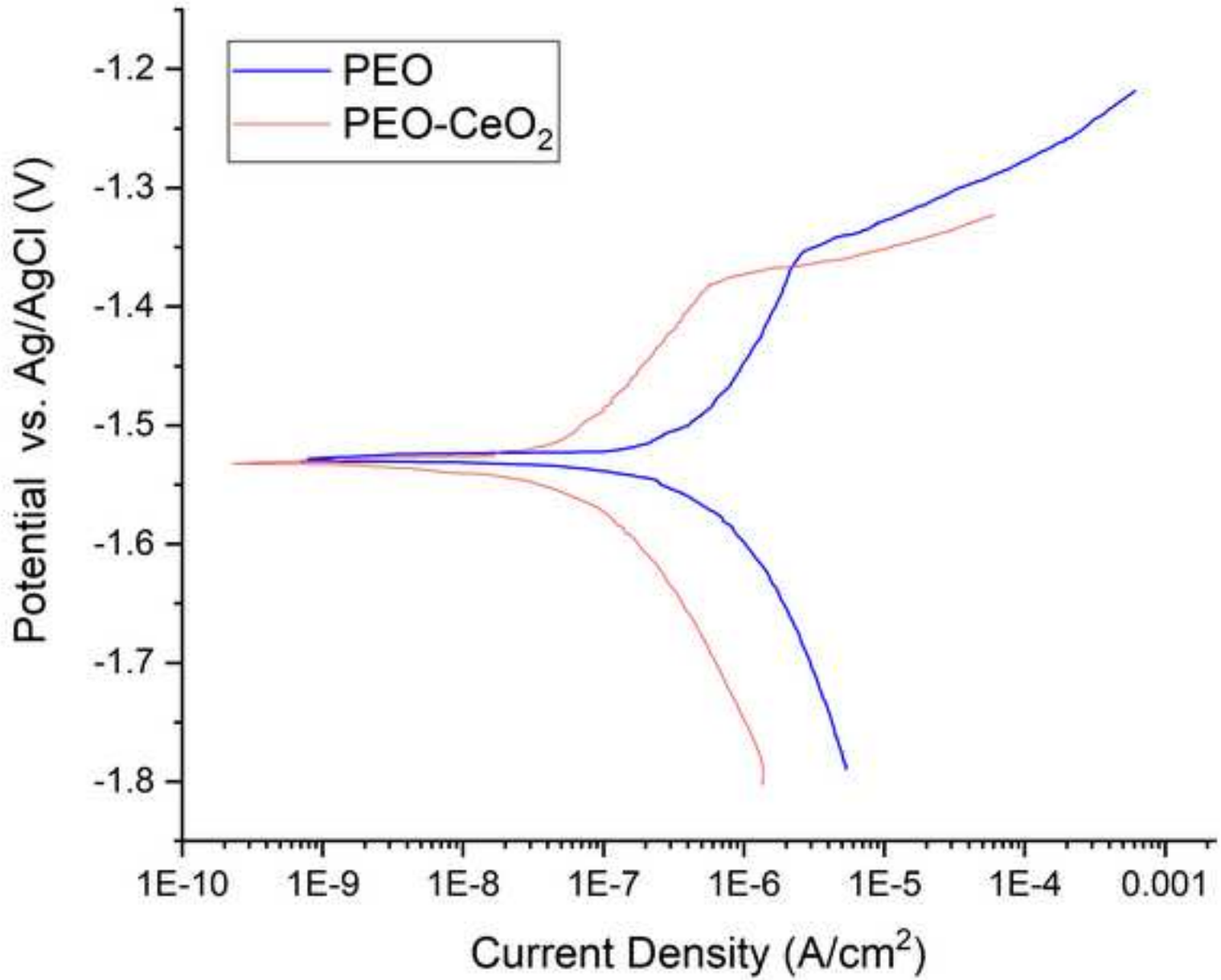

Figure 16

Click here to download high resolution image

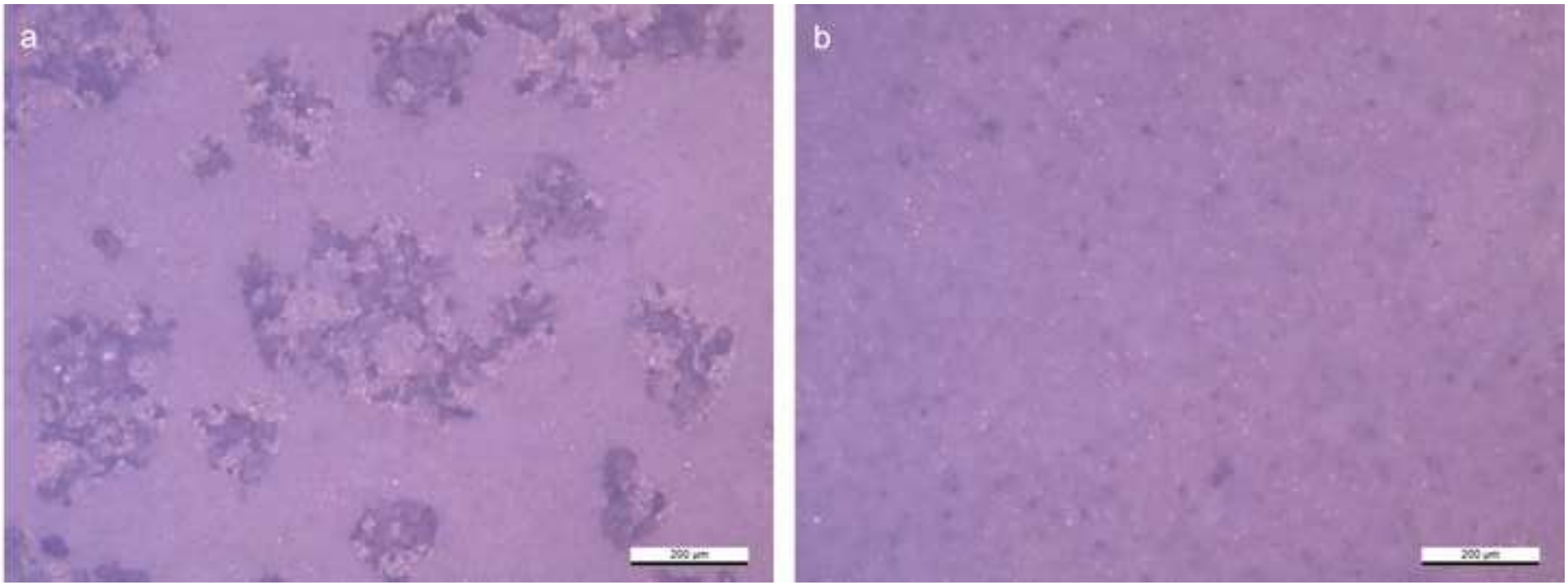

Suggested Reviewers

1- Dr. P. Bala Srinivasan,
SASTRA University, GE Global Research, GKSS Forschungszentrum, NIT-Trichy
pbs@nitt@edu

2- MetinUsta
ustam@gyte.edu.tr
Department of Materials Science and Engineering, Gebze Institute of Technology, Gebze, Kocaeli 41400, Turkey

3- Arash Fattah-alhosseini
Associate Professor of Materials Engineering, Bu-Ali Sina University, Iran
a.fattah@basu.ac.ir